JEM

Article

Plasmacytoid dendritic cells protect from viral bronchiolitis and asthma through semaphorin 4a–mediated T reg expansion

Jason P. Lynch,[1,9,10,18] Rhiannon B. Werder,[1,18] Zhixuan Loh,[1,5] Md. Al Amin Sikder,[1,18] Bodie Curren,[1,18] Vivian Zhang,[1,18] Matthew J. Rogers,[1] Katie Lane,[1] Jennifer Simpson,[1,18] Stuart B. Mazzone,[1,11] Kirsten Spann,[6,7] John Hayball,[12,13] Kerrilyn Diener,[12,13] Mark L. Everard,[14] Christopher C. Blyth,[14,15,16,17] Christian Forstner,[4] Paul G. Dennis,[4] Nida Murtaza,[8] Mark Morrison,[8] Páraic Ó Cuív,[8] Ping Zhang,[18] Ashraful Haque,[2,18] Geoffrey R. Hill,[2,18] Peter D. Sly,[2,3] John W. Upham,[8] and Simon Phipps[1,2,18]

[1]School of Biomedical Sciences, [2]Australian Infectious Diseases Research Centre, [3]Child Health Research Centre, [4]School of Earth and Environmental Sciences, and [5]The Institute for Molecular Bioscience, The University of Queensland, St. Lucia, Queensland, Australia
[6]School of Biomedical Science and [7]Institute of Health and Biomedical Science, Queensland University of Technology, Brisbane, Queensland, Australia
[8]The University of Queensland Diamantina Institute, The University of Queensland, Translational Research Institute, Woolloongabba, Queensland, Australia
[9]Department of Medicine, Division of Infectious Diseases, Massachusetts General Hospital, Cambridge, MA
[10]Department of Microbiology and Immunobiology, Harvard Medical School, Boston, MA
[11]Department of Anatomy and Neuroscience, The University of Melbourne, Melbourne, Victoria, Australia
[12]School of Pharmacy and Medical Sciences, University of South Australia, Adelaide, South Australia, Australia
[13]Robinson Research Institute, Adelaide Medical School, The University of Adelaide, Adelaide, South Australia, Australia
[14]School of Medicine, University of Western Australia, Perth, Western Australia, Australia
[15]Department of Infectious Diseases and [16]Department of Microbiology, PathWest Laboratory Medicine WA, Princess Margaret Hospital for Children, Perth, Western Australia, Australia
[17]Wesfarmers Centre of Vaccines and Infectious Diseases, Telethon Kids Institute, University of Western Australia, Perth, Western Australia, Australia
[18]QIMR Berghofer Medical Research Institute, Herston, Queensland, Australia

Respiratory syncytial virus–bronchiolitis is a major independent risk factor for subsequent asthma, but the causal mechanisms remain obscure. We identified that transient plasmacytoid dendritic cell (pDC) depletion during primary Pneumovirus infection alone predisposed to severe bronchiolitis in early life and subsequent asthma in later life after reinfection. pDC depletion ablated interferon production and increased viral load; however, the heightened immunopathology and susceptibility to subsequent asthma stemmed from a failure to expand functional neuropilin-1^{+} regulatory T (T reg) cells in the absence of pDC-derived semaphorin 4a (Sema4a). In adult mice, pDC depletion predisposed to severe bronchiolitis only after antibiotic treatment. Consistent with a protective role for the microbiome, treatment of pDC-depleted neonates with the microbial-derived metabolite propionate promoted Sema4a-dependent T reg cell expansion, ameliorating both diseases. In children with viral bronchiolitis, nasal propionate levels were decreased and correlated with an IL-6^{high}/IL-10^{low} microenvironment. We highlight a common but age-related Sema4a-mediated pathway by which pDCs and microbial colonization induce T reg cell expansion to protect against severe bronchiolitis and subsequent asthma.

INTRODUCTION

Severe respiratory syncytial virus (RSV)–bronchiolitis is a major cause of morbidity and mortality in infants globally (Nair et al., 2010) and a major independent risk factor (i.e., in the absence of atopy) for asthma (extensively reviewed in Feldman et al. [2015]). A recent population study examining two large cohorts estimated that 13% of all asthma cases stem from RSV-bronchiolitis in infancy (James et al., 2013), suggesting that a better understanding of the underlying mechanisms will identify opportunities for new preventative therapies. RSV-bronchiolitis primarily affects children aged under 2 yr (Hall, 2001), and asthma most often commences in childhood, highlighting a window of susceptibility in early life. This period coincides with the postnatal assembly of the microbiota (Yatsunenko et al., 2012; Planer et al., 2016), an event that is integral to the development of host physiology and immune cell maturation, including the differentiation of regulatory T (T reg) cells (Hooper et al., 2012; Arpaia et al., 2013; Furusawa et al., 2013). However, whether the

Correspondence to Simon Phipps: simon.phipps@qimrberghofer.edu.au

The Rockefeller University Press
J. Exp. Med. 2018 Vol. 215 No. 2 537–557
https://doi.org/10.1084/jem.20170298

age-related development of the microbiota affects susceptibility to RSV-bronchiolitis remains unknown.

In response to respiratory virus infection, plasmacytoid dendritic cells (DCs [pDCs]) are recruited to the lungs and produce vast amounts of antiviral IFNα and IFNβ downstream of TLR7 activation (Swiecki and Colonna, 2015). Notably, pDCs contribute to T reg cell development in both thymus and periphery (de Heer et al., 2004; Martín-Gayo et al., 2010), and hence contribute to immunoregulation. Numbers of circulating pDCs in infancy are inversely correlated with lower respiratory tract infections and physician-diagnosed asthma at school age (Silver et al., 2009; Upham et al., 2009), and in vitro studies with peripheral blood mononuclear cells show that pDCs limit type 2 cytokine production after stimulation with a respiratory virus (Pritchard et al., 2012). RSV does not infect pDCs or affect pDC survival, but it can impair IFN production (Hornung et al., 2004; Schlender et al., 2005; Guerrero-Plata et al., 2006; Schijf et al., 2013). Antibody-mediated depletion of pDCs increases the magnitude of type 2 inflammation to RSV infection in adult mice, although this phenotype was not ameliorated by IFNα administration (Smit et al., 2006; Wang et al., 2006). Intriguingly, T reg cell function is impaired in RSV-bronchiolitis (Raiden et al., 2014; Christiaansen et al., 2016), and in neonatal mice, RSV infection was shown to diminish tolerance via an effect on T reg cells (Krishnamoorthy et al., 2012). *TLR7* polymorphisms are linked to asthma risk, and TLR7 hyporesponsiveness is evident in subjects with asthma (Møller-Larsen et al., 2008; Roponen et al., 2010). Infection with pneumonia virus of mice (PVM), a mouse-specific Pneumovirus of the same genus as RSV, in the absence of *Tlr7* predisposes to severe bronchiolitis in mice, whereas the adoptive transfer of *Tlr7*-sufficient pDC to *Tlr7*-deficient mice confers protection (Davidson et al., 2011). Moreover, secondary infection induced the cardinal features of asthma, including airway hyperreactivity (AHR), airway remodeling (e.g., smooth muscle hyperplasia), and airway inflammation (Kaiko et al., 2013). Collectively, these findings suggest that the nexus between severe bronchiolitis and subsequent asthma is underpinned by perturbations to the pDC compartment (Lynch et al., 2014), although whether pDCs mediate protection via antiviral cytokines, T reg cells, or both remains ill defined.

Here we used BDCA2-diptheria toxin receptor (DTR) transgenic mice (Swiecki et al., 2010) to induce the specific and temporal depletion of pDCs during primary PVM infection alone. In neonatal, but not adult, mice, pDC depletion increased bronchiolitis severity and was sufficient to evoke an asthma-like phenotype upon viral challenge. In adult mice, pDC depletion was insufficient to induce severe bronchiolitis, unless the microbiota was perturbed, suggesting that host–commensal interactions are protective. In both age groups, bronchiolitis was associated with a failure to expand neuropilin-1 $(Nrp\text{-}1)^+$ T reg cells, caused by the absence of pDC-expressed semaphorin 4a (Sema4a). Supplementation of pDC-depleted neonates with the microbial metabolite propionate increased the number of Sema4a-expressing monocyte-derived DCs (moDCs), expanded $Nrp\text{-}1^+$ T reg cells, and conferred protection against severe viral bronchiolitis and subsequent asthma. Sema4a blockade attenuated the protective effects of propionate, including the expansion of $Nrp\text{-}1^+$ T reg cells, suggesting that pDCs and the microbiome confer resistance through a common pathway. Similarly, we found a $propionate^{low}$ $IL\text{-}10^{low}$ $IL\text{-}6^{high}$ phenotype in 2-yr-old children with viral bronchiolitis. Together, our findings highlight a common but age-related Sema4a-mediated pathway by which pDC and microbial colonization confer protection against severe bronchiolitis and subsequent asthma.

RESULTS

pDC depletion predisposes toward severe PVM–induced bronchiolitis in neonatal but not adult mice

Several studies have implicated a key role for pDCs in controlling the severity of RSV infection by using anti-BST2 (also known as PDCA-1 or clone 120G8) to deplete pDCs (Smit et al., 2006; Wang et al., 2006). However, because type I and II IFNs up-regulate the expression of BST2 on other immune cells, this approach is potentially confounded. In contrast, the BDCA2-DTR transgenic mouse strain allows for the specific and inducible depletion of pDCs during the course of infection (Swiecki et al., 2010). To address the role of pDCs during acute respiratory viral infection in early life, we first sought to determine whether diphtheria toxin (DT) exposure would deplete pDCs in the lungs and mediastinal lymph nodes (MLN) of BDCA2-DTR neonates. To test this, 6-d-old BDCA2-DTR transgene–positive (hereafter pDC^{Δ}) and negative (WT) littermates were exposed to a single, low dose of DT (3,000 ng/kg body weight, i.p.), and pDCs ($CD11b^-$, $B220^+$, $CD11c^+$, $Siglec\text{-}H^+$, $CD45RA^+$) were assessed 24 h later by flow cytometry. Using this protocol, pDCs were >85% lower in pDC^{Δ} neonates compared with their WT counterparts (Fig. S1 a). In contrast, lung myeloid DCs ($MHCII^{hi}$, $CD11c^{hi}$, $CD11b^+$, $B220^-$) were unaffected by DT treatment (not depicted). In line with previous studies (Swiecki et al., 2010), a dose of 6,000 ng/kg was required to deplete pDCs in the lungs and MLN of pDC^{Δ} adult mice. To evaluate whether pDC depletion predisposes to severe viral bronchiolitis, and whether susceptibility was age-related, 1- and 6-wk-old pDC^{Δ} and WT littermates were inoculated with low-dose PVM (10 plaque-forming units [PFU], i.n.) or vehicle (10% FCS/DMEM), treated with DT (irrespective of genotype) at −1, 1, 3, and 5 d postinfection (dpi) and killed at 7 and 10 dpi (Fig. 1 a). Vehicle-inoculated mice were treated with DT and killed at 10 dpi. At 7 dpi, the peak of pDC infiltration to the PVM-infected lung (Davidson et al., 2011; Kaiko et al., 2013; Edwards et al., 2015), pDCs were significantly lower in the lungs and MLN of pDC^{Δ} neonates and pDC^{Δ} adults (Fig. 1, b and c), but had recovered by 10 dpi (Fig. S1 b). Consistent with a critical role for pDCs in the generation of innate antiviral cytokines during acute PVM infection in early life (Davidson et al., 2011; Kaiko et al.,

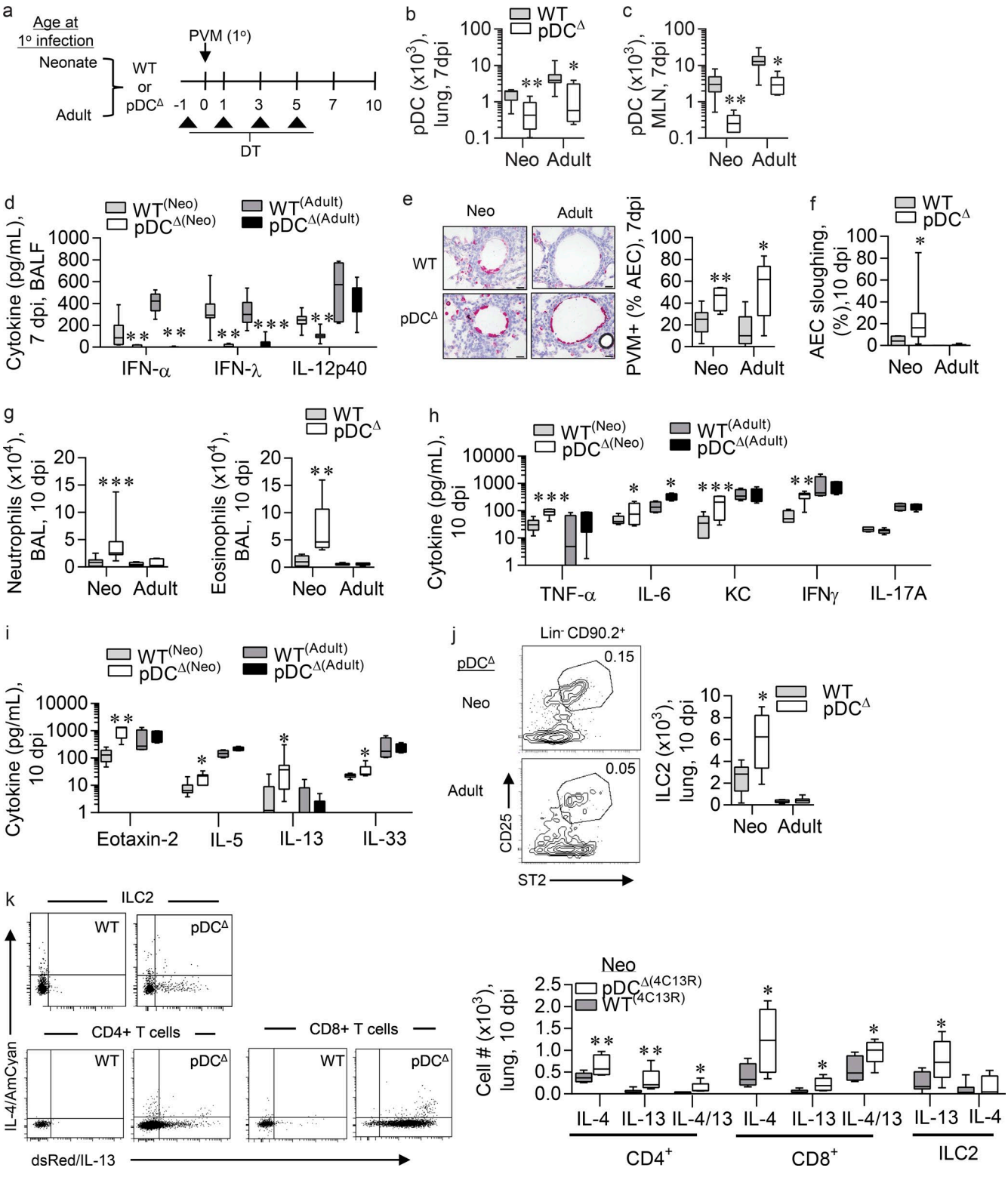

Figure 1. **pDC depletion predisposes toward severe PVM-induced bronchiolitis and subsequent asthma in neonatal but not adult mice. (a)** Study design. 1-wk-old (neo) or 6-wk-old (adult) pDC$^{\Delta}$ and WT mice were treated with DT (i.p. route, 15 ng) at −1, 1, 3, and 5 dpi, inoculated with PVM or vehicle at 0 dpi, and killed at 7 and 10 dpi. **(b and c)** pDC (CD11b^{-} B220^{+} CD11c^{+} Siglec-H^{+} CD45RA^{+}) number in lung (b) and MLNs (c). **(d)** IFN-α, IFN-λ, and IL-12p40 protein expression in BALF. **(e)** Representative micrograph (x1000 magnification) of PVM immunoreactivity in the airway epithelium, and quantification of PVM positive AECs. Bars, 50 µm. **(f)** Quantification of AEC sloughing. **(g)** Neutrophil and eosinophil numbers in BAL. **(h)** Proinflammatory

2013), IFNα and IFNλ levels in the bronchoalveolar lavage fluid (BALF) were >100-fold lower in both neonatal and adult pDC$^{\Delta}$ mice compared with age-matched WT mice (Fig. 1 d and Fig. S1 c). As expected, pDC depletion increased the viral load in the airway epithelium, the primary site of Pneumovirus replication. In WT neonatal and adult mice, PVM G protein expression peaked at 7 dpi (Figs. 1 e and S1 d), then fell to fewer than 5% of airway epithelial cells (AECs) by 10 dpi. In contrast, twice as many AECs were PVM positive in both pDC$^{\Delta}$ neonates and adults at 7 dpi (Fig. 1 e and Fig. S1 d). Moreover, both neonatal and adult pDC$^{\Delta}$ mice exhibited a marked delay in viral clearance at 10 dpi.

AEC detachment is a feature of viral bronchiolitis and is associated with disease severity and viral load (Johnson et al., 2007). In our model, AEC sloughing was significantly elevated in neonatal pDC$^{\Delta}$ compared with WT mice, but was absent in adult pDC$^{\Delta}$ and WT mice (Fig. 1 f and Fig. S1 e). Weight loss was similar between pDC$^{\Delta}$ and WT adults, whereas pDC$^{\Delta}$ neonates exhibited stunted weight gain compared with WT controls (not depicted), suggestive of a hyper-inflammatory response in the pDC$^{\Delta}$ neonates. Indeed, airway neutrophilia and eosinophilia was evident in neonatal but not adult pDC$^{\Delta}$ mice (Fig. 1 g and Fig. S1 f). The expression of IL-6 was elevated at 10 dpi in both neonatal and adult pDC$^{\Delta}$ mice relative to age-matched WT mice, whereas the levels of TNF-α, KC (CXCL1), and IFN-γ were significantly elevated in pDC$^{\Delta}$ neonates but not pDC$^{\Delta}$ adult mice (Fig. 1 h and Fig. S1 g). Collectively, these data suggest that pDCs are critical for antiviral cytokine production and viral control in both neonatal and adult mice, but only in the neonatal period are pDCs necessary to temper the magnitude of the inflammatory response.

Severe bronchiolitis is often associated with an elevated type 2 inflammatory response (Bendelja et al., 2000; Sheppard et al., 2003; Caballero et al., 2015). When compared with age-matched WT littermates, the levels of eotaxin-2 (CCL24), IL-5, IL-13, and IL-33 (but not IL-4, TSLP, or IL-25; not depicted) were significantly elevated at 10 dpi in neonatal, but not adult pDC$^{\Delta}$ mice (Fig. 1 i and Fig. S1 h). The elevated expression of IL-5 and IL-13 but not IL-4 implicated a potential role for type 2 innate lymphoid cells (ILC2s), and indeed ILC2 (Lineage^{-} CD90.2^{+} CD25^{+} ST2^{+}) numbers were significantly elevated in the lungs of pDC$^{\Delta}$ neonates compared with pDC$^{\Delta}$ adult mice, WT neonates, and WT adults (Fig. 1 j and Fig. S1 i). To identify the cellular source of IL-13, we crossed pDC$^{\Delta}$ mice with 4C13R reporter mice, which express AmCyan fluorescent protein under the control of the IL-4 promoter and dsRed fluorescent protein under the control of the IL-13 promoter (Huang et al., 2015). As with pDC$^{\Delta}$ neonatal mice, double transgenic pDC$^{\Delta(4C13R)}$ neonatal mice developed severe bronchiolitis (not depicted). In the lungs, we found that ILC2s, together with CD4^{+} Th2 cells and CD8^{+} Tc2 cells, were the major source of IL-13 in neonatal pDC$^{\Delta}$ mice (Fig. 1 k). Total numbers of lung and MLN CD4 and CD8 T cells (Fig. S1 j) and the levels of IL-17A in BALF (Fig. 1 h and Fig. S1 k) were not significantly different between pDC$^{\Delta}$ and WT at either age.

Severe bronchiolitis in early life predisposes to subsequent asthma upon viral challenge

The severity of RSV-bronchiolitis is a major independent risk factor for asthma (Feldman et al., 2015), and so we hypothesized that if RSV bronchiolitis were causal, pDC depletion in early life alone would be sufficient to predispose toward subsequent asthma in later life. To test this, mice that had experienced severe viral bronchiolitis (pDC$^{\Delta}$ neonates) or had been asymptomatic (WT neonates) in early life were challenged with PVM at 7 wk of age (Fig. 2 a). Noninfected vehicle groups for each genotype served as controls. Consistent with our hypothesis, only mice that had experienced severe viral bronchiolitis (pDC$^{\Delta}$) in infancy exhibited airway resistance at 7 d after viral challenge (Fig. 2 b). When we examined the lungs for pathological features of asthma, again only the mice that had experienced severe viral bronchiolitis in early life developed the cardinal features of asthma, including airway smooth muscle (ASM) remodeling, mucus plugging, and type 2 inflammation (airway eosinophilia, type 2 cytokine expression (IL-4 and IL-13) and periostin deposition (Fig. 2, c and d; and Fig. S2, a–d). With the exception of AHR, all pathologies of asthma were present only after viral challenge (Fig. S1 e), and hence were not merely a consequence of the primary infection. Further, the asthma-like pathologies were not related to an altered type 1 or type 17 inflammatory response (Fig. S2, c and d), PVM-specific antibody levels (Fig. S2 f), or changes in lung pDC numbers during viral challenge (Fig. S2 g).

Using pDC$^{\Delta(4C13R)}$ mice, we observed that CD4^{+} Th2 cells were the dominant source of IL-13 in the lungs, although IL-13–producing CD8^{+} Tc2 cells were also significantly elevated in the MLN of pDC$^{\Delta(4C13R)}$ mice (Fig. S2 h). IL-4/IL-13 expression was restricted to T lymphocytes, consistent with the absence of ILC2 expansion in the lungs at 1, 3, or 7 d after viral challenge (not depicted). Collectively, these results suggest that severe viral bronchiolitis in early life is causally linked to virus-provoked eosinophilic asthma in later life.

pDC support the expansion of Nrp-1^{+} T reg cells and IL-10 production in the lung during early-life PVM infection

pDCs have been reported to support T reg cells (de Heer et al., 2004; Sharma et al., 2007; Palomares et al., 2012), and hence

cytokine production in lung tissue. **(i)** Type-2 cytokine production in BALF. **(j)** Representative flow cytometry plots and number of type 2 ILCs in lung. Quadrants display percentage of parent population. **(k)** Representative flow cytometry plots and numbers of IL-13 (dsRed) and IL-4 (AmCyan) expressing type 2 ILCs, CD4^{+} and CD8^{+} T cells in lungs of WT/4C13R and pDC$^{\Delta}$/4C13R mice at 10 dpi. Data are representative of $n = 2$ experiments with 6–8 mice per group and presented as box-and-whisker plots showing quartiles (boxes) and range (whiskers). Data were analyzed using one-way ANOVA with Tukey's post hoc test; *, $P < 0.05$; **, $P < 0.01$; ***, $P < 0.001$.

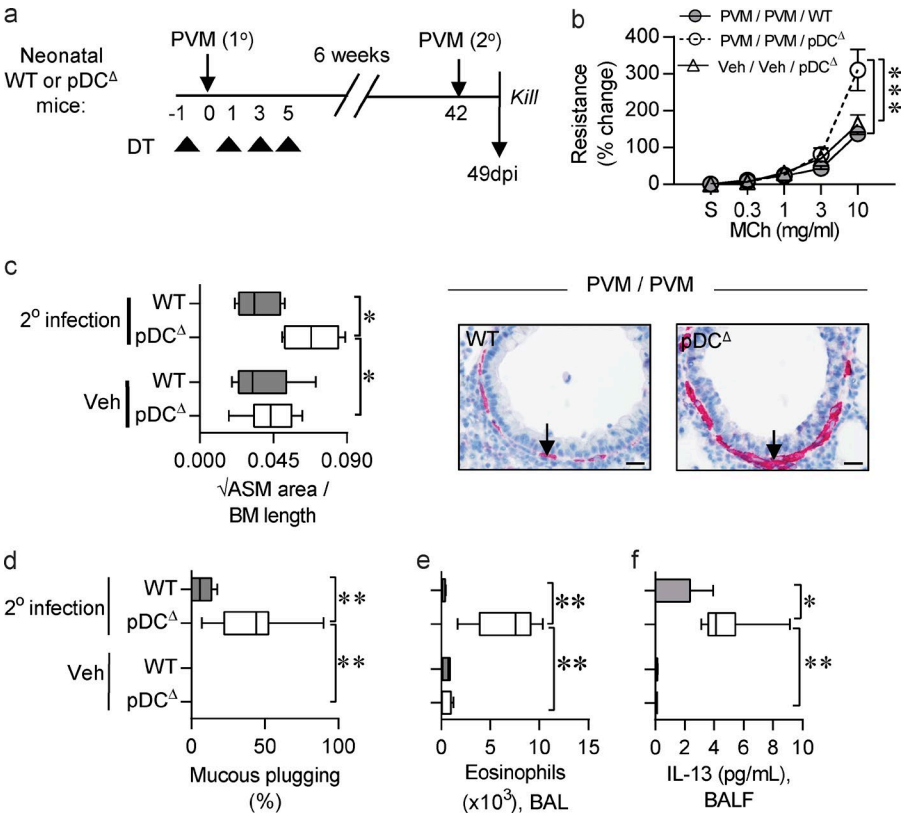

Figure 2. **Severe bronchiolitis in early life predisposes to subsequent asthma. (a)** Study design. 1-wk-old (neo) or 6-wk-old (adult) pDC$^{\Delta}$ and WT mice were treated with DT (i.p. route, 15 ng) at −1, 1, 3, and 5 dpi, inoculated with PVM or vehicle at 0 dpi, challenged with PVM at 42 dpi, and killed at 49 dpi. **(b)** AHR. **(c)** ASM area. Representative micrographs of ASM (400× magnification); arrows indicate ASM (pink). Bars, 50 µm. **(d)** Airway intraluminal mucus plugging. **(e)** Eosinophils in BAL. **(f)** IL-13 protein expression in BALF. Data are representative of $n = 2$ experiments with five to six neonates in each group and are presented as mean ± SEM (b) or box-and-whisker plots showing quartiles (boxes) and range (whiskers; c–f). Data were analyzed by two-way ANOVA (b) or one-way ANOVA (c–f) with Tukey's post hoc test; *, $P < 0.05$; **, $P < 0.01$; ***, $P < 0.001$.

we questioned whether severe bronchiolitis was a consequence of insufficient immunoregulation. Because the overexuberant inflammatory response peaked at 10 dpi (Fig. 1, g–i), we first quantified T reg cells in the lungs and MLNs at 5, 7, and 10 dpi. Probing the lungs with anti-FoxP3 by immunohistochemistry revealed that in WT mice, FoxP3$^+$ cells were widely distributed and sparse in number at baseline, but rapidly increased at 7 dpi and persisted until at least 10 dpi. In contrast, there was a negligible increase in FoxP3$^+$ cells in pDC$^{\Delta}$ mice (Fig. 3 a). Using flow cytometry, we confirmed our immunohistochemical findings and identified that the vast majority (>80%) of the T reg cells (CD3$^+$, CD4$^+$, CD25$^+$, FoxP3$^+$) were positive for neuropilin-1 (Nrp-1; Fig. 3 b) and Helios (not depicted), putative markers of thymic T reg cells (Weiss et al., 2012; Yadav et al., 2012). In the MLN, Nrp-1$^+$ T reg cell expansion began at 5 dpi (2 d before their increase in the lung) and peaked at 7–10 dpi (Fig. 3 c): this response was significantly diminished in pDC$^{\Delta}$ neonates. In contrast, the numbers of FoxP3$^-$ CD4$^+$ conventional T cells (T con) and FoxP3$^-$ CD8 T con in the lung and MLN were unaltered by pDC depletion (Fig. S1 j). To assess Nrp-1$^+$ T reg cell proliferation in the MLN in vivo, we injected the mice with BrdU. The frequency of BrdU$^+$ T reg cells was significantly lower in pDC$^{\Delta}$ compared with WT neonates, at both 7 and 10 dpi (Fig. 3 d). Notably, the failure to expand T reg cells in pDC$^{\Delta}$ mice coincided with the period pDCs would normally infiltrate the lungs and MLN (Fig. 3, e and f) and was not associated with altered Nrp1 expression (Fig. 3 b). The level of MHC-II expression on pDCs was increased in response to PVM infection (~2-fold in the MLN and ~5-fold in the lung; Fig. 3 g), although whether pDCs were actively presenting PVM antigens to the T reg cells remains to be demonstrated.

The levels of IL-10, an immunoregulatory cytokine secreted by T reg cells, was elevated in the lungs of infected WT mice but not pDC$^{\Delta}$ neonates (Fig. 3 h). Double transgenic pDC$^{\Delta}$/IL-10-GFP$^+$ mice revealed that pDC depletion primarily affected T reg cell and CD4$^+$ T con cell IL-10 production (Fig. 3 h). The expression of active TGF-β1, another immunoregulatory cytokine, was similarly diminished at 10 dpi in pDC$^{\Delta}$ neonates but not at earlier time points (not depicted). Moreover, examination of several functional surface markers on T reg cells revealed that the nucleotidase CD39 was markedly lower on lung Nrp-1$^+$ T reg cells from pDC$^{\Delta}$ neonates compared with their WT counterparts (Fig. 3 i). Collectively, our data indicate that pDCs contribute to the expansion and functional maturation of Nrp-1$^+$ T reg cells during Pneumovirus infection in early life.

pDC expression of Sema4a expands Nrp-1$^+$ T reg cells during early-life PVM infection

To address whether pDCs directly support T reg cell expansion, pDCs were purified from the MLN of WT neonates and co-cultured at a 1:40 ratio with CFSE-labeled CD4$^+$ T cells purified from the MLN of pDC$^{\Delta(4xDT)}$ neonates (Fig. 4 a). In the absence of pDCs, stimulation with α-CD3 alone did not increase the level of T reg proliferation, as measured by

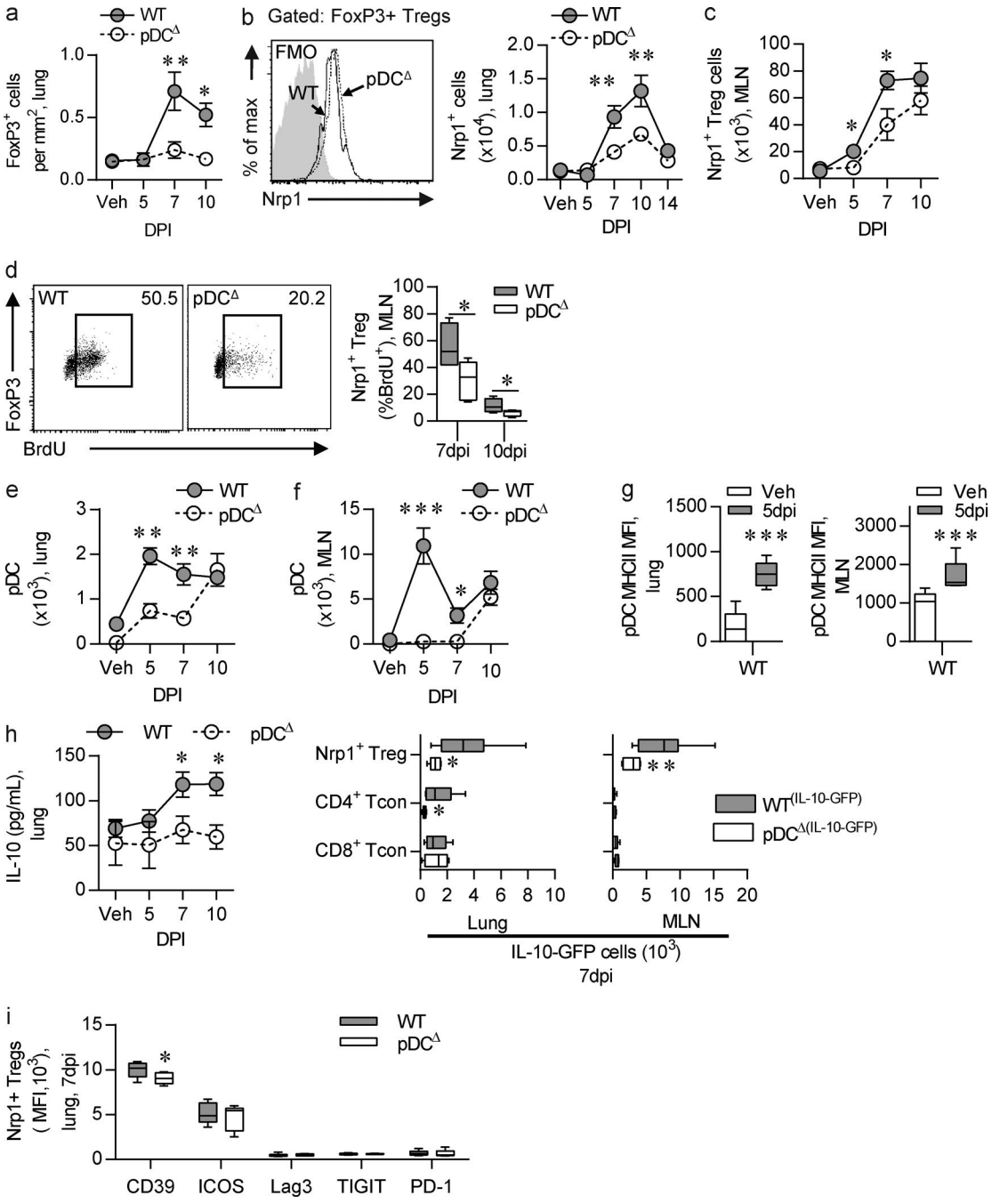

Figure 3. **pDC depletion diminishes the expansion of Nrp-1$^+$ T reg cells and IL-10 production in the lung during early-life PVM infection. (a)** FoxP3$^+$ cells enumerated in lung tissue sections. **(b)** Histogram of Nrp-1 expression on T reg cells (gated on CD4$^+$ CD3ε^+ CD25$^+$ CD25$^+$ Foxp3$^+$; top) and number of Nrp-1$^+$ T reg cells in lung (bottom). **(c)** Number of Nrp-1$^+$ T reg cells in MLN. **(d)** Representative flow cytometry plots of BrdU expression by Nrp1$^+$ T reg cells in MLN. **(e and f)** Proliferating BrdU/Nrp-1$^+$ T reg cells in MLN. Kinetics of pDC number in lung (e) and MLN (f). **(g)** MHCII expression on pDCs. **(h)** IL-10 protein expression in lung (left) and IL-10-GFP$^+$ cells in lung (middle) and MLN (right). **(i)** Immune-suppressive expression on Nrp-1$^+$ T reg cells in lung. Data are representative of $n = 2$ experiments with four to six neonates in each group and are presented as mean ± SEM (a–c and f) or as box-and-whisker plots showing quartiles (boxes) and range (whiskers; d, f, and g). Data were analyzed by one-way ANOVA with Tukey post hoc test (a–f and h) or Mann–Whitney *U* test (g, h [right], and i); *, $P < 0.05$; **, $P < 0.01$; ***, $P < 0.001$ compared with the WT control group.

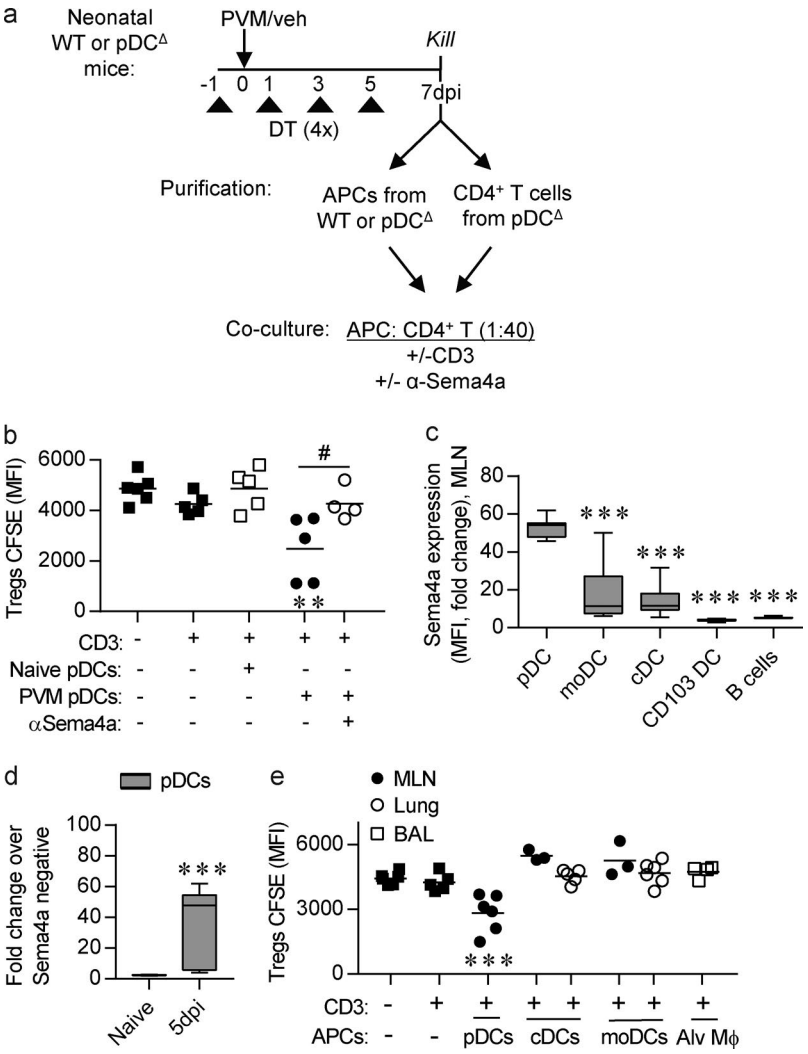

Figure 4. **pDC expression of Sema4a expands Nrp-1^{+} T reg cells during early-life PVM infection. (a)** Protocol for APC and CD4^{+} T cell co-culture. **(b and e)** Mean fluorescence intensity of CFSE in Nrp1^{+} T reg cells. **(c)** Sema4a expression on MLN APCs at 7 dpi. **(d)** Sema4a expression on MLN pDCs. For panels b and e, each data point represents a technical replicate and is representative of $n = 2$ independent experiments. For panels c and d, data are representative of $n = 2$ independent experiments with four to six neonates in each group and are presented as box-and-whisker plots showing quartiles (boxes) and range (whiskers). Data were analyzed by one-way ANOVA with Tukey post hoc test (b, c, and e) or Mann–Whitney *U* test (d); #, $P < 0.05$; **, $P < 0.01$; ***, $P < 0.001$ compared with unstimulated cells (b and e), pDCs (c), naive group (d), or as indicated.

a decrease in CFSE intensity, compared with the unstimulated cells (Fig. 4 b). When stimulated in the presence of pDCs from PVM-infected but not naive WT mice, there was a significant increase in FoxP3^{+} Nrp1^{+} T reg cell proliferation. Blockade with anti-Sema4a significantly reduced this response (Fig. 4 b), suggesting that pDCs provide the cognate ligand for Nrp-1, recently identified as Sema4a (Delgoffe et al., 2013). Strikingly, surface expression of Sema4a was markedly higher on pDCs compared with other antigen-presenting cells in the MLN (Fig. 4 c), the site of T reg cell expansion (Fig. 3, c and d), and was increased after PVM infection (Fig. 4 d). Notably, other prototypical APCs, including conventional DCs (cDCs), moDCs, and alveolar macrophages sourced from infected pDC-depleted neonates, were insufficient to induce T reg cell proliferation (Fig. 4 e).

Blockade of Sema4a but not IFNαR1 signaling increases bronchiolitis severity and predisposes to subsequent asthma

To specifically address whether pDCs protect against severe viral bronchiolitis via the production of antiviral cytokines or the expansion of T reg cells, we treated PVM-infected WT neonates with anti-Sema4a or anti-IFNαR to block Sema4a-Nrp-1 or type I IFN signaling, respectively (Fig. 5 a). As expected, anti-IFNαR but not anti-Sema4a diminished IFN-α expression and increased viral burden (Fig. 5, b and c), while not affecting pDC numbers (not depicted). In contrast, Sema4a, but not IFN-αR, blockade significantly decreased T reg cell numbers, proliferation, and CD39 expression, as well as IL-10 levels in the lung (Fig. 5, d–f). Critically, perturbing the T reg cell response but not type I IFN signaling led to increased AEC sloughing, granulocytic inflammation, and type 2 inflammation (Fig. 5, g–j), suggesting that Sema4a blockade in early life may be sufficient to predispose toward asthma in later life. To assess this, we repeated the early-life treatment with anti-Sema4a during primary infection and then challenged with PVM 6 wk later. Similar to pDC depletion, Sema4a blockade in early life alone was sufficient to induce the hallmark features of asthma in later life (Fig. 5, k–o). Collectively, these findings suggested that a failure to generate Nrp-1^{+} T reg

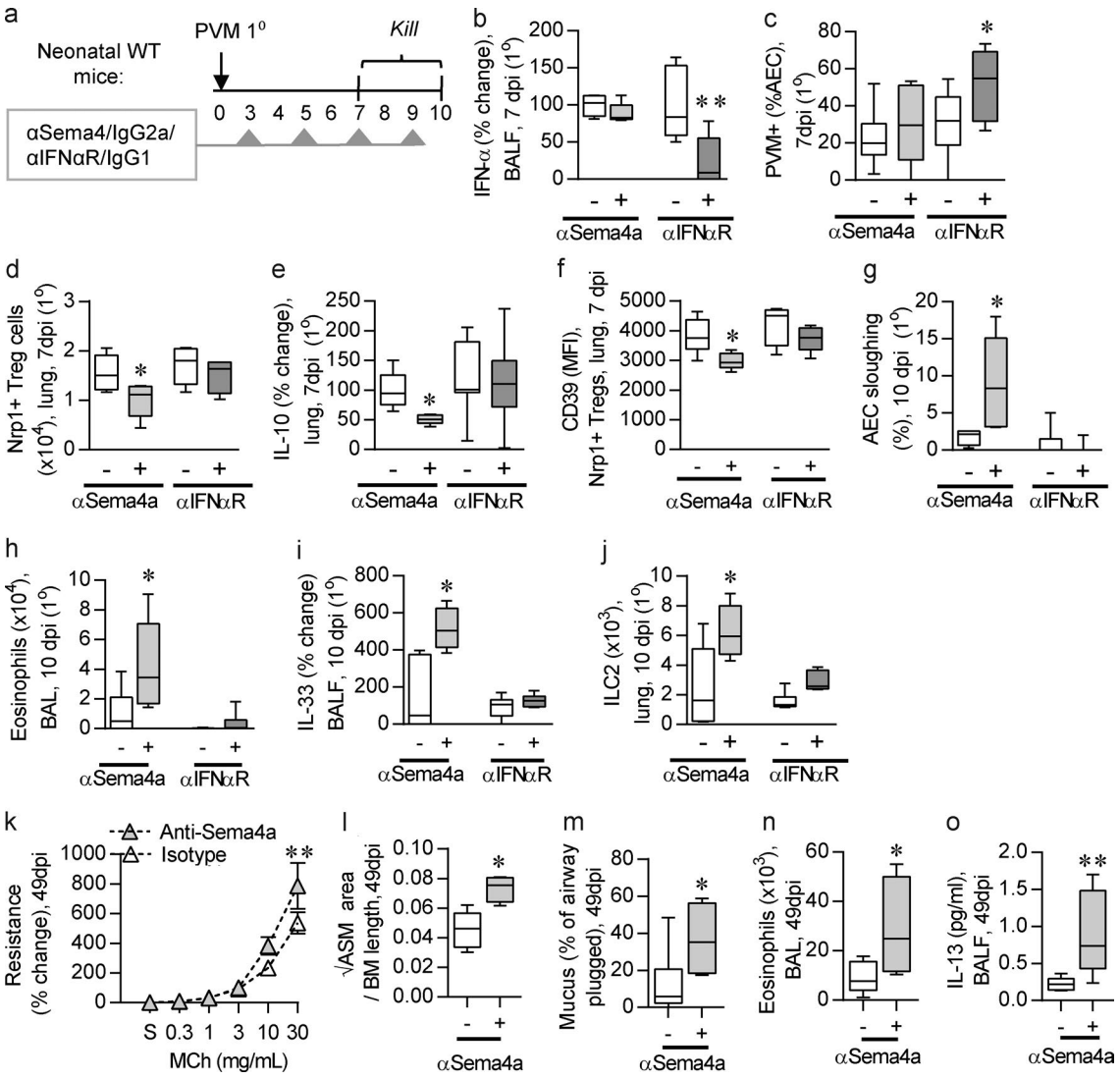

Figure 5. **Blockade of Sema4a but not IFNαR1 signaling increases bronchiolitis severity and predisposes to subsequent asthma. (a)** Protocol of PVM inoculation and administration of αSema4a or isotype control (IgG2a) and αIFNαR or isotype control (IgG1) to neonatal WT mice. **(b)** IFN-α protein expression in BALF, expressed as % change of the respective isotype control. **(c)** Viral load in the airway epithelium. **(d)** Nrp-1$^+$ T reg cells in the lung. **(e)** IL-10 protein expression in lung, expressed as % change of the respective isotype control. **(f)** CD39 expression by Nrp-1$^+$ T reg cells. **(g)** Sloughing of the airway epithelium. **(h)** Eosinophil number in BAL. **(i)** IL-33 protein expression in lung, expressed as % change of the respective isotype control. **(j)** Type-2 ILCs in lung. **(k)** AHR. **(l)** ASM area. **(m)** Intraluminal mucus plugging. **(n)** Eosinophil number in BAL. **(o)** IL-13 protein expression in BAL. Data are representative of $n = 2$ experiments with four to six neonates in each group and are presented as the mean ± SEM (k) or box-and-whisker plots showing quartiles (boxes) and range (whiskers; b–o). Data were analyzed by one-way (b–j and l–o) or two-way (k) ANOVA with Tukey's post hoc test; *, $P < 0.05$; **, $P < 0.01$ compared with the respective isotype control–treated group or as indicated.

cells in early life predisposes toward both severe bronchiolitis and subsequent asthma.

Nrp-1$^+$ T reg cell transfer prevents the development of PVM-induced bronchiolitis and subsequent asthma

To confirm the importance of T reg cells, we next isolated Nrp-1$^+$CD4$^+$FoxP3$^+$ T reg or T con (CD4$^+$FoxP3$^-$) cells from the MLN of PVM-infected FoxP3-RFP mice and adoptively transferred 30,000 cells (i.p. route) to pDC$^\Delta$ neonates at 5 dpi (Fig. 6 a), simulating the time of T reg expansion (Fig. 3 c). The transfer of T reg but not T con cells significantly decreased AEC sloughing, IL-6 production, granulocytic inflammation, IL-13 and IL-33 levels, and nuclear-to-cytoplasmic translocation of HMBG1 in AECs in early life (Fig. 6, b–h). Of note, neither T reg nor T con cell transfer affected viral load (Fig. 6 i). Consistent with a causal role for RSV-bronchiolitis in the onset of postviral asthma in later life, the restoration of Nrp-1$^+$ T reg cells in early life was sufficient to protect against viral challenge–induced asthma (Fig. 6, j–m). Antigen-specific T reg cells are superior

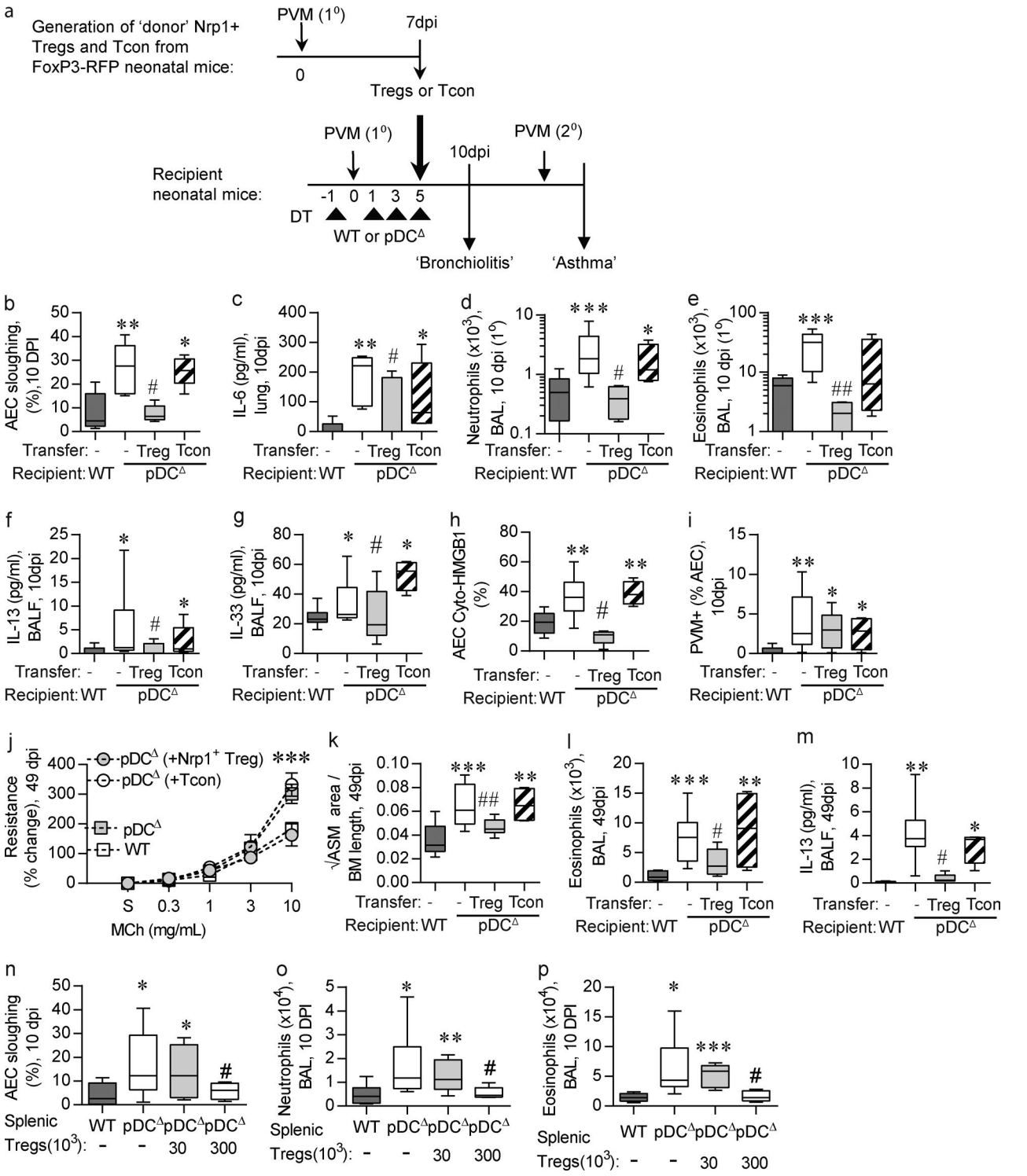

Figure 6. **Nrp-1⁺ T reg cell restoration prevents the development of PVM-induced bronchiolitis. (a)** Protocol of acute PVM infection/pDC depletion and Nrp-1⁺ T reg adoptive transfer 5 dpi (30,000 Nrp-1/Foxp3-RFP⁺ T reg cells, Foxp3-RFP⁻ T con or vehicle diluent; intranasal route). **(b and n)** Sloughing of the airway epithelium. **(c)** IL-6 protein expression in the lung. **(d and o)** Neutrophil number in BAL. **(e, l, and p)** Eosinophil number in BAL. **(g)** IL-33 expression in BALF. **(h)** Nuclear to cytoplasmic HMGB1 translocation in AECs. **(f and m)** IL-13 expression in BALF. **(i)** Viral load in the airway epithelium. **(j)** AHR. **(k)** ASM area. Data are representative of $n = 2$ experiments with four to six neonates in each group and are presented as the mean ± SEM (j) or box-and-whisker plots showing quartiles (boxes) and range (whiskers; b–i and k–p). Data were analyzed by one-way (b–i and k–p) or two-way (j) ANOVA with Tukey's post hoc test; *, $P < 0.05$; **, $P < 0.01$; ***, $P < 0.001$ compared with WT mice or as indicated; #, $P < 0.05$; ##, $P < 0.01$ compared with pDC$^{\Delta}$ mice.

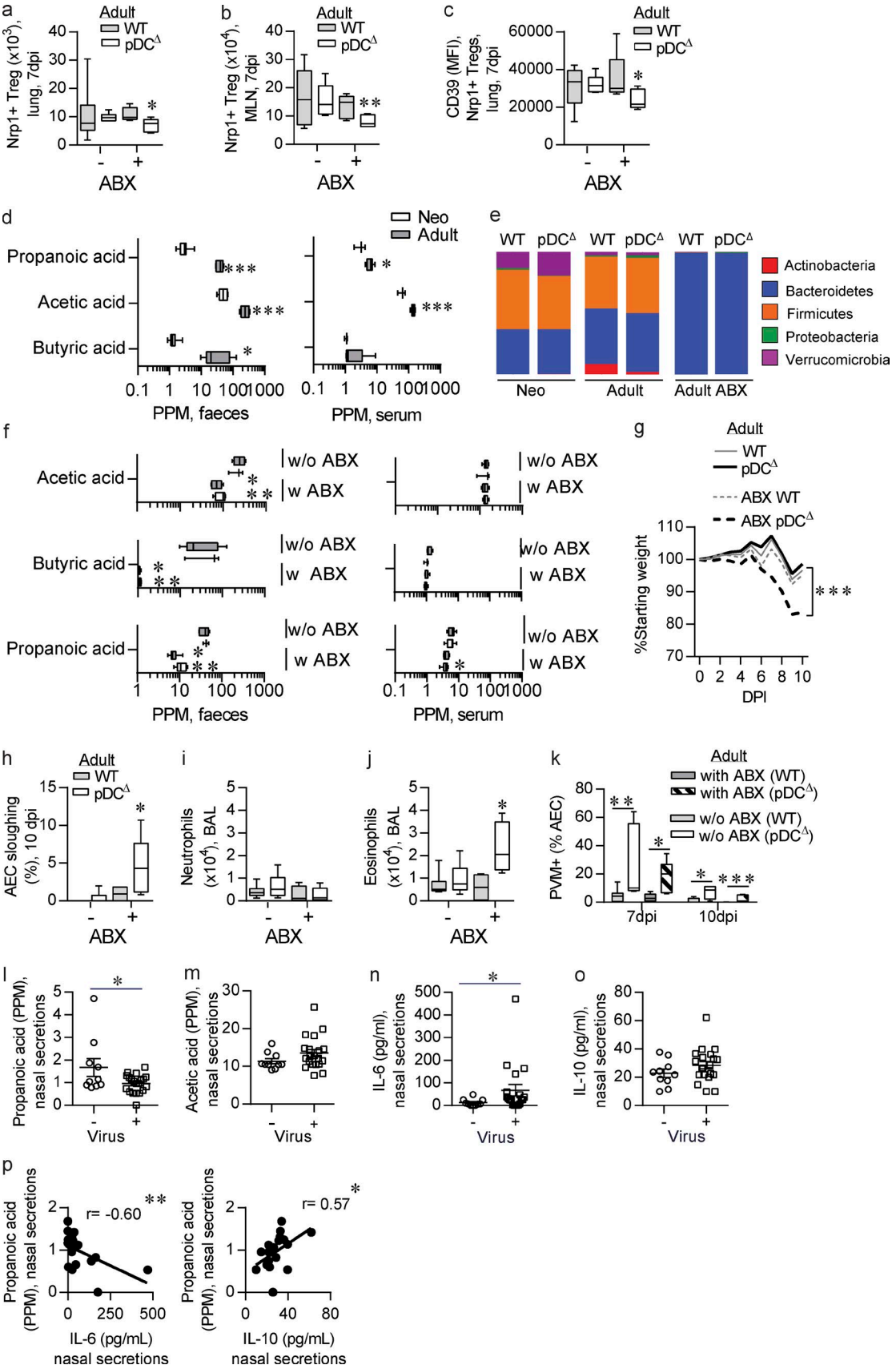

to polyclonal T reg cells in their suppressor capacity (Tarbell et al., 2007). Hence, in an attempt to address antigen specificity of the Nrp1$^+$ T reg cells, we next assessed the efficacy of splenic T reg cells. Unlike the T reg cells isolated from the MLN, the adoptive transfer of 30,000 splenic Nrp1$^+$ T reg cells from PVM-infected neonatal mice was not sufficient to confer protection (Fig. 6, n–p). However, consistent with the ability of T reg cells to suppress inflammation in a nonspecific manner, the transfer of 300,000 cells did ameliorate disease severity in pDC$^\Delta$ neonates (Fig. 6, n–p).

Microbial colonization in adult mice confers resistance to viral bronchiolitis

The fundamental role of T reg cells in protecting against severe RSV-bronchiolitis in infants (Figs. 3 and 4), together with the age-dependent nature of disease susceptibility (Fig. 1), suggested that in adult mice, the expansion of T reg cells is less dependent on pDCs. Consistent with this notion, PVM infection of adult pDC$^\Delta$ mice had no effect on the numbers of Nrp-1$^+$ T reg cells in the lungs or MLN, nor did it effect their expression of CD39 (Fig. 7, a–c) or Nrp1 (not depicted). Recent insights have revealed that microbial metabolites, such as the short-chain fatty acids (SCFAs) propanoic acid, acetic acid, and butyric acid, shape host immunity by promoting the differentiation of T reg cells (Arpaia et al., 2013; Furusawa et al., 2013). This led us to hypothesize that the postnatal assembly of the microbiota, which is complete by 6 wk of age in mice (Pantoja-Feliciano et al., 2013; Gollwitzer et al., 2014), may confer protection in older mice through the expansion of T reg cells. As expected, the levels of SCFAs propanoic acid, acetic acid, and butyric acid were significantly greater in adults compared with neonatal mice in both fecal pellets and serum, with the exception of serum butyrate levels (Fig. 7 d). The gut microbiota of WT and pDC$^\Delta$ neonates was similar: both were dominated by bacteria affiliated with the Firmicutes (*Lactobacillus* spp.), Bacteroidetes (Bacteroidales S24-7, *Bacteroides* spp. and *Parabacteroides* spp.), and Verrucomicrobia (*Akkermansia* spp.; Fig. 7 e and Fig. S3 a). The gut microbiota of WT and pDC$^\Delta$ adult mice was also similar, and although bacteria affiliated with the Firmicutes (*Lactobacillus* spp. and *Allobaculum* spp.) and Bacteroidetes (Bacteroidales S24-7) were again dominant, there was a reduction in bacteria affiliated with the Verrucomicrobia (*Akkermansia* spp.) and an increase in bacteria affiliated with the Actinobacteria (*Bifidobacterium* spp. and *Adlercreutzia* spp.) compared with neonatal mice (Fig. 7 e and Fig. S3 a). Treatment of pDC$^\Delta$ and WT adult littermates with broad-spectrum antibiotics (ABX; vancomycin, neomycin, ampicillin, metronidazole) for 6 wk (Russell et al., 2012; Moon et al., 2015) led to a dramatic and similar reduction in diversity, and to a community dominated by bacteria affiliated with *Parabacteroides* spp. (Fig. 7 e). Moreover, the levels of propanoic acid, acetic acid, and butyric acid in the fecal pellets in mice of both genotypes and serum propanoic acid in pDC$^\Delta$ mice were significantly decreased (Fig. 7 f and Fig. S3 a). Notably, ABX treatment of pDC$^\Delta$ mice, but not WT mice, significantly attenuated the expansion of T reg cells in the lungs and MLN, as well as their expression of CD39 (Fig. 7, a–c), leading to a marked increase in weight loss, AEC sloughing, and eosinophilic inflammation, without affecting viral burden (Fig. 7, g–k).

Nasal SCFA propanoic acid levels inversely correlate with a proinflammatory milieu in human viral bronchiolitis

We next explored whether our findings were relevant to human disease by analyzing samples from children recruited as part of an influenza vaccine effectiveness study (Table S1). Of those with viral bronchiolitis, 10 of 20 subjects were positive for RSV. In the absence of fecal or serum samples, we compared SCFAs and cytokine levels in the nasal secretions of infants with viral or nonviral bronchiolitis. Strikingly, the levels of SCFA propanoic acid were significantly lower in infants with viral bronchiolitis compared with nonviral bronchiolitis (Fig. 7 l). In contrast, the levels of acetic acid and butyric acid did not differ between the groups (Fig. 7 m and Fig. S3, b and c). In the children with viral (but not nonviral) bronchiolitis, expression of proinflammatory IL-6 was significantly increased in the nasal secretions (Fig. 7 n). Although the expression of anti-inflammatory IL-10 was not different (Fig. 7 o), we found that propanoic acid levels negatively correlated with the expression of IL-6 and positively correlated with anti-inflammatory IL-10 (Fig. 7 p and Fig. S3 c).

Exogenous SCFA propionate confers protection against severe bronchiolitis and subsequent asthma in pDC-depleted neonatal mice

Our findings suggested that the lower levels of SCFAs in neonatal pDC$^\Delta$ mice contribute to the age-dependent sus-

Figure 7. **Microbial colonization in adult mice confers resistance to viral bronchiolitis. (a–c)** Nrp-1$^+$ T reg cell number in lung (a) and MLN (b) and CD39 expression (c). **(d)** SCFA levels in feces (left) and serum (right) of neonatal and adult WT mice. **(e)** Relative abundance of bacterial phyla. **(f)** SCFA levels in WT and pDC$^\Delta$ mice treated with broad-spectrum ABX or vehicle. **(g)** Weight loss over the course of PVM infection. **(h)** Airway epithelium sloughing. **(i)** Neutrophil number in BAL. **(j)** Eosinophil number in BAL. **(k)** Viral load in the airway epithelium. **(l)** Propanoic acid levels in the nasal secretions of human subjects with nonviral (n = 10) or viral (n = 20) bronchiolitis. **(m)** Acetic acid levels in the nasal secretions. **(n)** IL-6 expression in the nasal secretions. **(o)** IL-10 expression in the nasal secretions. **(p)** Correlations between SCFA propanoic acid and IL-6 (left) and IL-10 (right) in infants with viral bronchiolitis. Data are representative of n = 2 experiments with four to six mice in each group and presented as box-and-whisker plots showing quartiles (boxes) and range (whiskers; a–d, f, h–k) or mean ± SEM (i–o) or as individual subjects (p). Data were analyzed by one-way (a–c and h–k) or two-way (g) ANOVA with Tukey's post hoc test or Mann–Whitney U test (d and l) or Spearman's rank-order correlation (p); *, $P < 0.05$; **, $P < 0.01$; ***, $P < 0.001$ compared with neonatal mice, without ABX WT mice, or as indicated. See also Table S1.

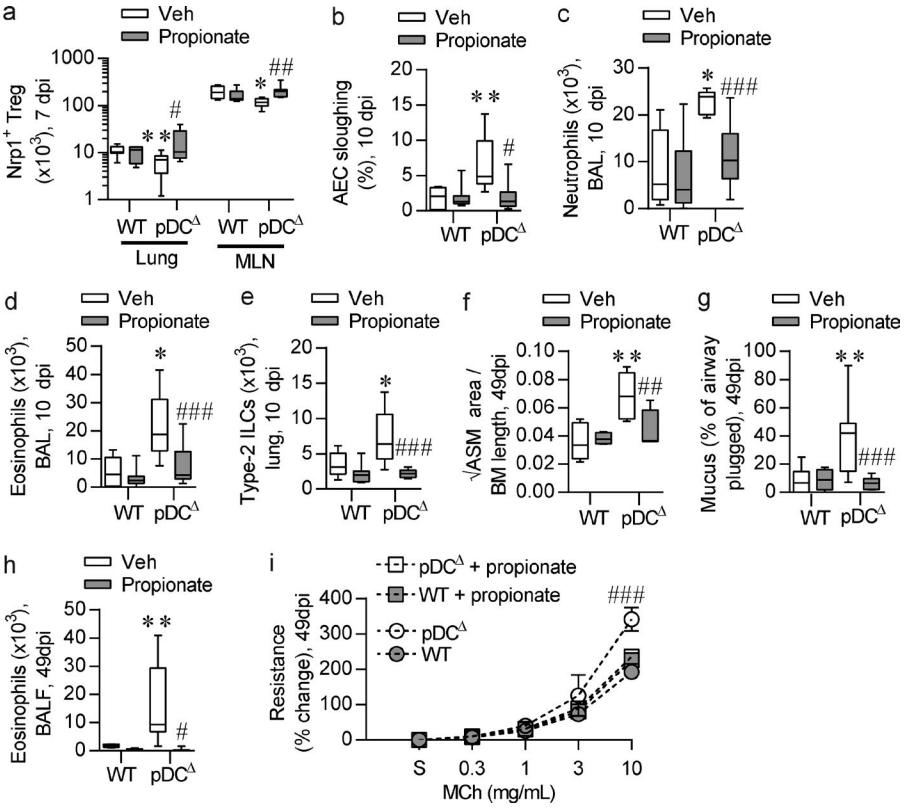

Figure 8. **Exogenous SCFA propionate confers protection against severe bronchiolitis and subsequent asthma in pDC-depleted neonatal mice through a Sema4a-dependent mechanism. (a)** Nrp-1$^+$ T reg cells in lung and MLN. **(b)** Airway epithelium sloughing. **(c and d)** Neutrophil (c) and eosinophil (d) numbers in BAL. **(e)** Type-2 ILCs in the lung. **(f)** ASM area. **(g)** Intraluminal mucus plugging. **(h)** Eosinophil number in BAL. **(i)** AHR. Data are representative of $n = 2$ experiments with four to six neonates in each group and presented as the mean ± SEM (i) or box-and-whisker plots showing quartiles (boxes) and range (whiskers; a–h). Data were analyzed by one-way (a–h) or two-way (i) ANOVA with Tukey's post hoc test; *, $P < 0.05$; **, $P < 0.01$ compared with vehicle-treated WT mice; #, $P < 0.05$; ##, $P < 0.01$; ###, $P < 0.001$ compared with vehicle-treated pDC$^\Delta$ mice. See also Fig. S3.

ceptibility to severe bronchiolitis. To test this, we added SCFA propionate to the drinking water of pregnant dams and administered SCFA propionate i.p. to the pups (Fig. S3 d). This regimen led to serum propanoic acid levels that were comparable to adult mice (Fig. S3 e). Strikingly, the attenuated expansion of T reg cells in pDC$^\Delta$ neonates was completely restored by SCFA propionate supplementation (Fig. 8 a), which in turn ablated AEC sloughing and neutrophilic inflammation (Fig. 8, b and c), and protected against the development of type 2 inflammation (Fig. 8, d and e). Notably, these effects occurred independently of an alteration to IFN-α production (Fig. S3 f) or the number of pDCs (Fig. S3 g). Critically, treatment with SCFA propionate in early life alone was sufficient to prevent the development of virus-induced ASM remodeling, type 2 inflammation, and AHR in later life (Fig. 8, f–i).

SCFA propionate confers protection through a Sema4a-dependent mechanism

SCFAs promote colonic T reg cell differentiation both directly, by affecting the stability of FoxP3 (Tao et al., 2007; Arpaia et al., 2013; Furusawa et al., 2013), and indirectly, by affecting the function of DCs (Arpaia et al., 2013; Trompette et al., 2014). To assess whether the protective effect of SCFA propionate on pDC-depleted mice might be mediated through enhanced Sema4a-Nrp-1 signaling via an APC other than pDCs, we measured *Sema4a* mRNA in the lungs and observed a massive increase in both WT and pDC$^\Delta$ neonates after exposure to SCFA propionate (Fig. 9 a). Using flow cytometry, we identified that SCFA propionate exclusively increased the numbers of Sema4a$^+$ moDCs in the lungs and MLN of pDC$^\Delta$ mice and the MLN of WT mice (Fig. 9 b). Strikingly, when stimulated in the presence of moDCs from PVM-infected, but not naive, WT mice, there was a significant increase in T reg cell proliferation (Fig. 9 c). Blockade with anti-Sema4a significantly reduced this response, although the magnitude of the decrease was modest. To ascertain whether the protective effect of propionate was mediated via the provision of Sema4a, we next treated pDC$^\Delta$ mice with exogenous propionate in the presence of anti-Sema4a. Although anti-Sema4a did not affect the propionate-mediated increase in Sema4a$^+$ moDCs in the lung or MLN as expected (Fig. 10, a and b), it significantly decreased the expansion of T reg cells and abrogated the beneficial effects of propionate on CD39 expression (Fig. 10, b and c). Furthermore, perturbing the restoration of the T reg cell response led to an increase in AEC sloughing, granulocytic inflammation, and type 2 inflammation (Fig. 10, d–h) and predisposed toward virus-induced asthma (Fig. 10, i–l), consistent with an important role for Sema4a and downstream T reg cell expansion in conferring protection against severe bronchiolitis and subsequent asthma.

DISCUSSION

Severe RSV-bronchiolitis in infancy is a major risk factor for subsequent asthma; however, the immunological mech-

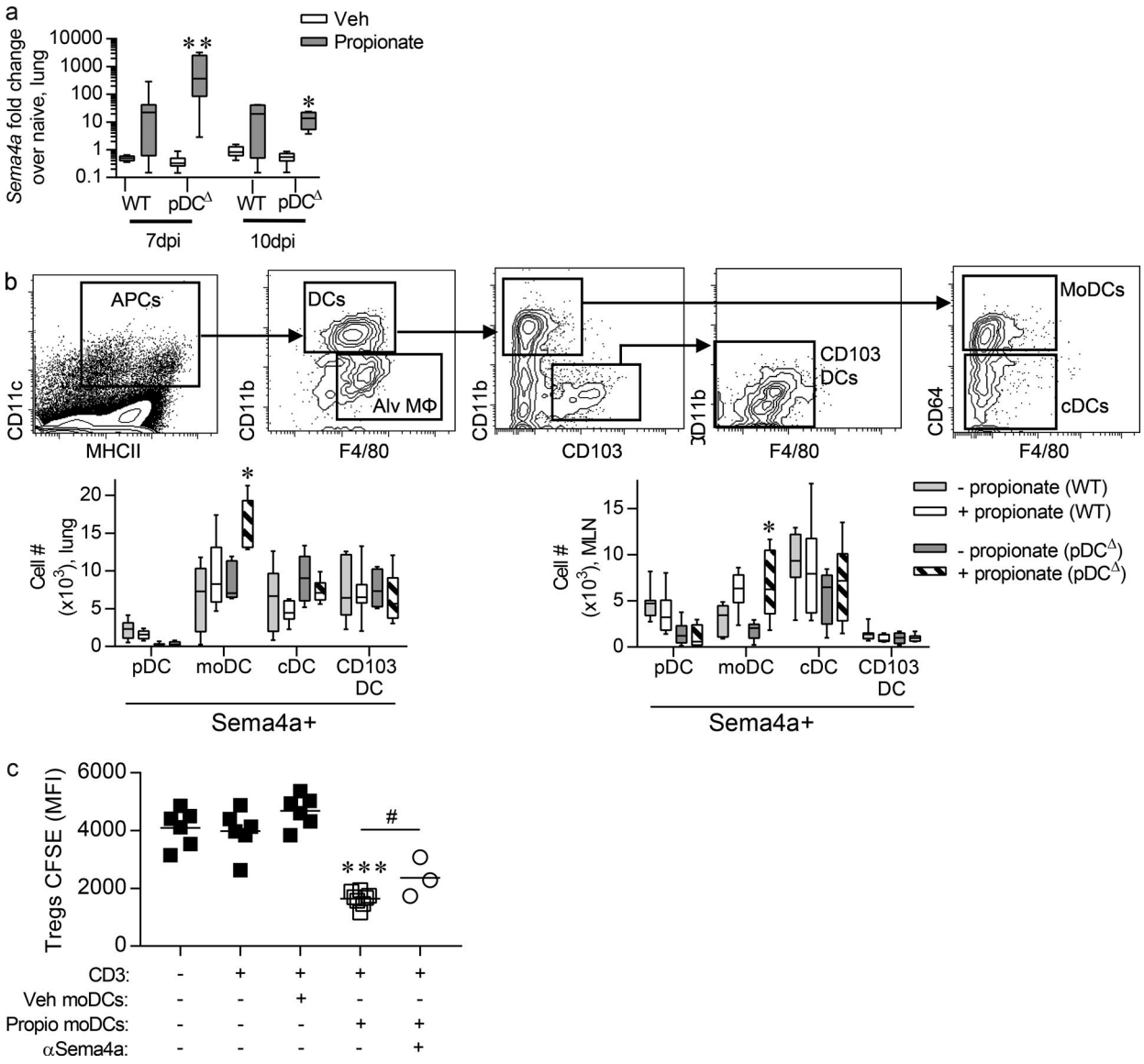

Figure 9. **Proprionate supplementation increases lung Sema4$^+$ moDCs. (a)** *Sema4a* mRNA expression in lung. **(b)** Sema4a-expressing DC numbers in lung (top) and MLN (bottom). Nrp-1$^+$ T reg cell number in lung. **(c)** Mean fluorescence intensity of CFSE in Nrp1$^+$ T reg cells. For panels a and b, data are representative of $n = 2$ experiments with four to six neonates in each group and are presented as box-and-whisker plots showing quartiles (boxes) and range (whiskers). For panel c, each data point represents a technical replicate and is representative of $n = 2$ experiments. Data were analyzed by one-way ANOVA with Tukey's post hoc test; *, $P < 0.05$; **, $P < 0.01$; ***, $P < 0.001$ compared with vehicle-treated pDC$^{\Delta}$ mice (a and b) or unstimulated cells (c).

anisms that underlie this association have remained elusive. Here we found that targeted pDC depletion during primary viral infection in infancy alone was sufficient to predispose to both severe bronchiolitis in early life and viral challenge–induced asthma in later life, suggesting causality. Consequent to pDC depletion, disease susceptibility was unrelated to the impaired antiviral IFN response; instead, it was underpinned by a failure to expand Nrp-1$^+$ T reg cells, which were required to limit immunopathology and the onset of type 2 inflammation. Moreover, we identified that the age-dependent susceptibility to viral bronchiolitis was related to microbial colonization: elevated levels of the microbial SCFAs in older mice facilitated the expansion of lung T reg cells, thus providing a redundant pathway in the absence of pDCs. Strikingly, SCFA propanoic acid levels were lower in the nasal secretions of young children with acute viral bronchiolitis compared with control subjects and inversely correlated with levels of immunoregulatory IL-10. Our findings implicate a causal role for RSV-bronchiolitis in asthma onset and highlight a new molecular pathway by which both microbial colonization and optimal pDC function support

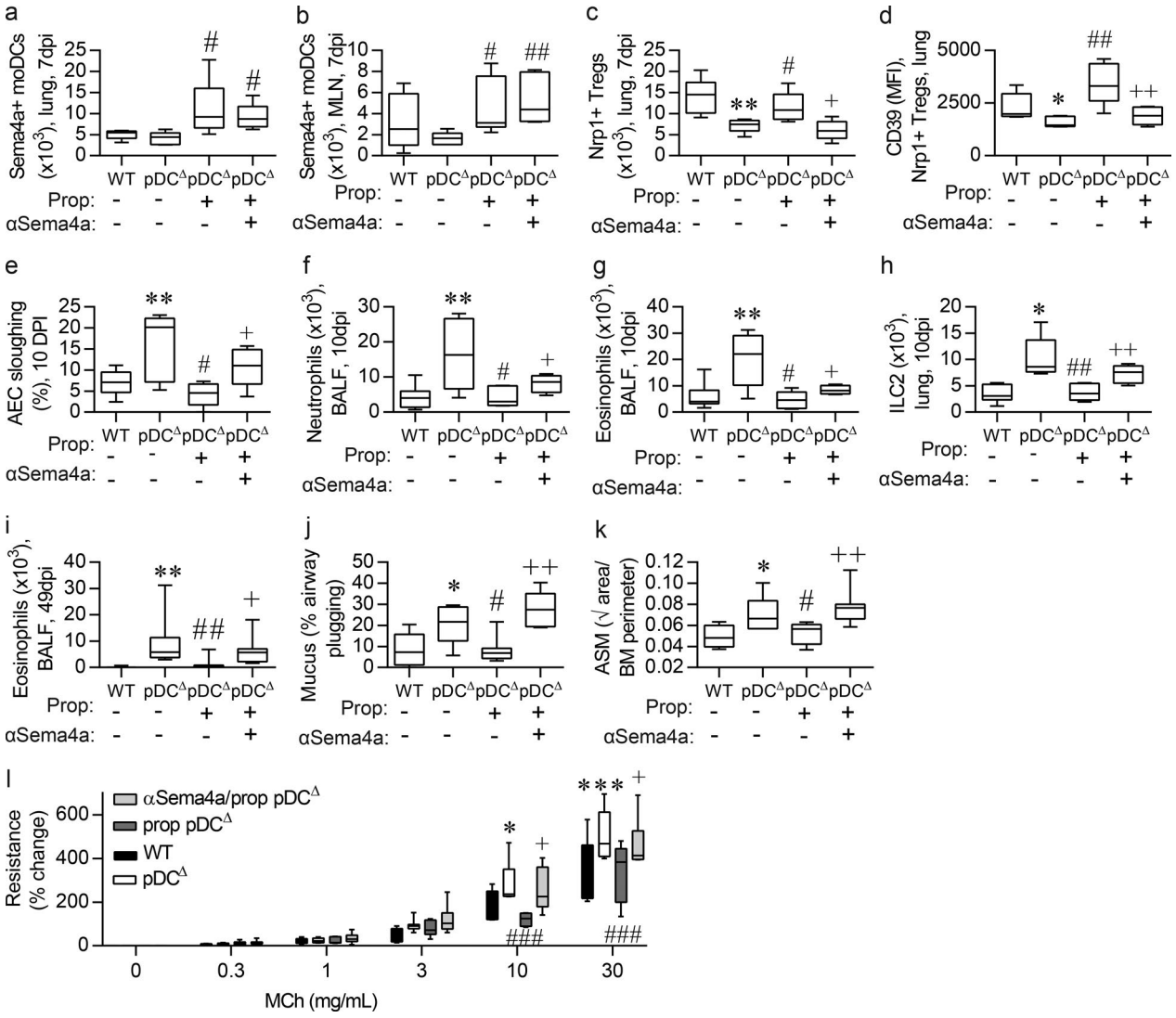

Figure 10. **Propionate supplementation confers protection via Sema4a. (a and b)** Sema4a-expressing moDC number in lung (a) and MLN (b). **(c)** Nrp1$^+$ T reg cells in lung. **(d)** CD39 expression on Nrp1$^+$ T reg cells in lung. **(e)** AEC sloughing. **(f)** Neutrophils in BALF. **(g and i)** Eosinophils in BALF. **(h)** ILC2s in lung. **(j)** Mucous production by AECs. **(k)** ASM growth. **(l)** AHR. Data are representative of $n = 2$ experiments with four to six neonates in each group and are presented as the mean ± SEM (l) or box-and-whisker plots showing quartiles (boxes) and range (whiskers; a–k). Data were analyzed by one-way (a–k) or two-way (l) ANOVA with Tukey's post hoc test *, $P < 0.05$; **, $P < 0.01$; ***, $P < 0.001$ compared with vehicle-treated pDC$^\Delta$ mice; $^\#$, $P < 0.05$; $^{\#\#}$, $P < 0.01$; $^{\#\#\#}$, $P < 0.001$ compared with vehicle-treated pDC$^\Delta$ mice; $^+$, $P < 0.05$; $^{++}$, $P < 0.01$ compared with propionate-treated pDC$^\Delta$ mice.

T reg cell expansion to confer resistance against severe RSV-bronchiolitis and subsequent asthma.

pDCs are able to produce considerable quantities of type I IFNs. Impaired antiviral immunity, particularly defective type I IFN production, has been linked to asthma pathogenesis, and low numbers of circulating pDCs in infancy are predictive of lower respiratory tract infections, wheezing, and asthma (Silver et al., 2009; Upham et al., 2009). In the present study, we found that whereas pDC depletion in neonatal mice diminished the production of IFNα/λ and increased viral load, blockade of the type I IFN receptor was not sufficient to cause AEC sloughing, which was routinely associated with severe neutrophilia. Rather, the increase in disease severity in pDC-depleted or anti-Sema4a–treated mice stemmed from a failure to support T reg cell expansion and the consequent loss of IL-10– and TGF-β–mediated immunoregulation. Critically, at the time of T reg cell expansion, the MLN were enriched with pDCs, and although other APCs also expressed Sema4a, it was most abundantly expressed on pDCs. Consistent with an important role for pDC-derived Sema4a, the aberrant T reg cell response was restricted to T reg cells expressing its cognate ligand, Nrp-1$^+$. Using an in vitro system, we demonstrated that pDCs directly mediated T reg cell expansion via Sema4a; in contrast, the other APC populations

that we tested did not promote T reg cell proliferation. We found that pDCs up-regulated MHCII, and that pDCs from infected and not naive mice promoted T reg cell proliferation in vitro. However, as our in vitro assay used agonistic anti-CD3, further studies are required to definitively demonstrate whether pDCs present specific antigen or merely serve as a nonspecific accessory cell by providing Sema4a and other cofactors to expand virus-specific T reg cells in this model. We identified that pDCs are necessary for optimal T reg cell function: both IL-10 production and CD39 expression were diminished in pDC-depleted mice, consistent with previous research demonstrating that Sema4a-Nrp1 signaling promotes the suppressive activity of T reg cells (Delgoffe et al., 2013). Notably, the failure to induce the expansion of fully functional Nrp-1$^+$ T reg cells led to an elevated type 2 response; conversely, the adoptive transfer of competent Nrp-1$^+$ T reg cells from infected WT mice attenuated bronchiolitis and suppressed type 2 inflammation and, moreover, prevented subsequent asthma in later life. Importantly, low T reg cell numbers are associated with RSV-bronchiolitis in infants (Raiden et al., 2014; Christiaansen et al., 2016), and although others have observed that T reg cells limit RSV-bronchiolitis in mice, our findings are the first to provide a cellular and molecular mechanism governing their expansion and activation. T reg cells have been shown to be aberrant in asthma; hence, future studies should address whether perturbations to pDC function contribute to the development of long-lived, dysfunctional T reg cells.

Infants are at greatest risk of severe RSV-associated morbidity and mortality (Nair et al., 2010), and in accordance with this, we found that pDC depletion in neonatal but not adult mice predisposed to severe bronchiolitis. In adult mice, pDC depletion attenuated innate antiviral immunity but did not ablate T reg cell expansion, suggesting the existence of a redundant pathway that develops with age. This led us to question whether the gut microbiota as the primary producer of SCFAs might drive this expansion. Consistent with the greater diversity of the gut microbiota, the levels of propanoic acid were several logs higher in the feces and serum of adult mice. To assess whether microbial colonization conferred protection, we treated mice with ABX during rearing, and although this decreased gut microbiota diversity and propanoic acid levels in both the feces and serum, it was only in conjunction with pDC depletion that the adult mice developed severe bronchiolitis. Notably, this phenotype was associated with a failure to expand Nrp-1$^+$ T reg cells, as had occurred in neonatal mice, suggesting that pDCs and SCFAs act through a common pathway. Our data suggest that in neonatal immunity, pDCs play a critical role in supporting T reg cell development until the nascent microbiota is assembled and able to support T reg cell differentiation through the production of metabolites such as SCFAs.

Strikingly, we found that propanoic acid levels were significantly lower in nasal secretions collected from 2-yr-old children with viral bronchiolitis. Moreover, these levels correlated with a pathogenic IL-6^{hi}, IL-10^{lo} cytokine microenvironment. A limitation of our study is that we did not have access to fecal or serum samples, and so it was not possible to discern whether the low levels of SCFA propionate stemmed from local alterations to the respiratory microbiota (Teo et al., 2015; Mansbach et al., 2016) or was reflective of intestinal dysbiosis. Notably, the latter can affect circulating SCFA levels, thereby influencing peripheral tissues such as the upper airways (Trompette et al., 2014). Furthermore, it remains unclear whether the low propionate levels in the RSV-infected infants was a cause or consequence of severe viral bronchiolitis; this question will need to be explored via a large prospective study. Nonetheless, our findings from the preclinical model suggest that strategies aimed at modulating or mimicking the microbiota will diminish the substantial mortality and morbidity caused by RSV. In a recent population study, it was estimated that severe RSV bronchiolitis causes ∼13% of asthma cases, which is notable because in our model protection against severe viral bronchiolitis with exogenous SCFA propionate served as an effective preventive treatment against the inception of asthma. Mechanistically, we observed that SCFA propionate was able to replace pDC-mediated support of Nrp-1$^+$ T reg cells by increasing the number of Sema4a-expressing moDCs in the lungs and MLN, potentially as a consequence of increased hematopoiesis in the bone marrow (Trompette et al., 2014). Notably, we found that Sema4a blockade ablated the protective effects of SCFA against bronchiolitis and subsequent asthma, and thus we identify a common pathway through which microbial-derived metabolites and pDCs mediate the expansion of T reg cells.

In developed nations, microbial dysbiosis is increasing because of changes in diet (i.e., a shift to higher fat/sugar and lower fiber content), increased sanitation, formula feeding, urban living, and other factors (Arrieta et al., 2015). In a recent study, lower intestinal microbial diversity in the first 1 mo of life was observed in children who develop asthma compared with healthy controls, and another reported lower abundance of distinct bacterial genera and alterations to fecal SCFA levels and other microbial metabolites at 3 mo of age (Abrahamsson et al., 2014; Arrieta et al., 2015). A picture is also emerging to suggest that the respiratory microbiome in early life impacts on severity of RSV bronchiolitis, recurrent wheezing and the development of asthma (Rosas-Salazar et al., 2016; Zhou et al., 2016), although none of these studies has yet interrogated whether such changes affect T reg cell differentiation. In mice, several investigators have shown that acute allergen-induced asthma is increased in germ-free or ABX-treated adult mice (Herbst et al., 2011; Hill et al., 2012; Russell et al., 2012), and neonatal mice are similarly predisposed to allergen-induced airway inflammation, as the core phyla are not established until 1 mo of life (Marsland and Gollwitzer, 2014; Trompette et al., 2014). Adult mice fed a low-fiber diet also exhibit exaggerated type 2 allergic responses be-

cause of an attenuated metabolome (Gollwitzer et al., 2014). Our study is the first to implicate an important role of the microbiome in protecting against viral bronchiolitis and the later inception of asthma.

In summary, we identified that in neonatal WT mice, pDCs are necessary to confer protection against severe bronchiolitis and subsequent asthma, and that this dependence is lost upon microbial acquisition in later life. SCFA propionate supplementation to pDC-depleted neonatal mice promoted the immigration of moDCs to the lung, refurbishing the Sema4a signal and restoring the Nrp-1$^+$ T reg cell response, and hence conferred protection against severe viral bronchiolitis and subsequent asthma. Strategies that favorably affect the acquisition of a diverse microbiota in early life, or supplementation with key microbial metabolites, are likely to be useful for the prevention of viral bronchiolitis and in breaking its connection with asthma.

MATERIALS AND METHODS

Mouse strains

C57BL/6 BDCA-2-DTR male mice (provided by M. Colonna, Washington School of Medicine, St. Louis, MO) were time mated with WT (Animal Resources Centre), C57BL/6 FoxP3-RFP (provided by C. Engwerda, QIMR Berghofer Medical Research Institute, Brisbane, QLD, Australia; Lin et al., 2005), C57BL/6 IL-10-GFP (Kamanaka et al., 2006), or C57BL/6 4C13R (Huang et al., 2015) females under specific pathogen–free conditions at the Australian Institute of Biotechnology and Nanotechnology Animal Facility. Neonatal mice were genotyped by standard PCR using primers against *hGH* (BDAC-2-DTR mice), forward 5′-GCCCCC GGGCAGCACAGCCACTGCCGGTCC-3′ and reverse 5′-GGCCAAGCGCTTGGGCACTGTTCCCTCCCT-3′; *Dsred* (4C13R mice), forward 5′-GCTCCAAGGTGTACG TGAAG-3′ and reverse 5′-GCTTGGAGTCCACGTAGT AG-3′; IL-10–GFP, mutant 5′-CCAAAAGACGGCAAT ATGGT-3′, common 5′-GTGTGTATTGAGTCTGCT GGAC-3′, and WT 5′-GTGTGGCCAGCCTTAGAATAG-3′; FoxP3-RFP mice, mutant 5′-GGAATGCTCGTCAAG AAGACAGG-3′, common 5′-CAAAACCAAGAAAAG GTGGGC-3′, and WT 5′-CAGTGCTGTTGCTGTGTA AGGGTC-3′. All experiments were approved by the University of Queensland Animal Ethics Committee.

PVM inoculation

Pneumonia virus of mouse stock J3666 was prepared as previously described (Davidson et al., 2011). 10 PFU PVM or vehicle diluent (DMEM/FBS, 10% vol/vol; Gibco) was administered i.n. on day 7 or 49 of life under light isoflurane-induced anesthesia. In some experiments, mice were reinfected with 100 PFU PVM on day 49 of life.

Mouse treatments

BDCA2-DTR transgene–positive (denoted pDC$^\Delta$) and –negative (denoted WT) littermates received a low dose (neonates, 3,000 ng/kg; adults, 6,000 ng/kg) DT (Calbiochem) by i.p. injection at −1, 1, 3, and 5 dpi. DT administration with these protocols did not induce any adverse effects or an immune response in the absence of infection. A concentrated aqueous solution of BrdU (10:1; Invitrogen) was administered i.p. at 3, 5, 7, 8, and 9 dpi. 10 µg α-Sema4a (clone 757129; R&D Systems) or isotype control (IgG2a; R&D Systems) and 50 µg αIFNαR or isotype control (IgG1) were administered i.p. at 3, 5, 7, and 9 dpi. ABX including 0.25 g/liter vancomycin, 0.5 g/liter neomycin, 0.5 g/liter ampicillin, and 0.5 g/liter metronidazole (Sigma-Aldrich) were provided continuously via water bottle for 6 wk starting at embryonic day 13. To make the ABX palatable, we supplemented control and antibiotic water with artificial sweetener (Equal).

Flow cytometry

The left lung lobe, the smallest postcaval lobe, and the mediastinal lymph nodes (MLN) were washed separately in PBS/2% FCS before mechanical dissociation using a pestle and a 70-µm cell strainer (BD Biosciences). Isolated single-cell suspensions were washed with PBS/2% FCS, and red blood cells were lysed using Gey's buffer. Cells were washed again, followed by incubation with anti-FcγRIII/II (Fc block) for 15 min at 4°C. Cells were stained using fluorescently labeled antibodies directed against CD45RA-PE (14.8), CD4-AF488 or CD4-V500 (RM4-5), Ly6G-FITC (1A8), CD8α-PerCP-Cy5.5 (53-6.7), Gr-1–AF488 (RB6-8C5), CD11b-AF488 (M1/70), B220-AF488 (RA36B2), B220-V500 (RA36B2; all BD Bioscience); CD64-BV421 (X54-5/7.1), MHCII APC-Cy7 (M5/114.15.2), CD103-PE (2E7), CD25-BV605 (PC61), CD3ε-AF488 (145.2CII), CD11c-AF488 (N418), CD19-AF488 (6D5), CD45-BV421 (30-F11), CD11b-BV421 (M1/70), ST-2–APC (DIH9; all BioLegend); neurophilin-1–PE or -AF488 (761705; R&D Systems); Helios-PE (22F6), CTLA-4–PE (UC10-4B9), CD39-PerCP-efluor710 (24DMS1), ICOS-PE (C398.4A), Lag3-PerCP-efluor710 (C9B7W), TIGIT-PE (GIGD7), PD-1–APC-780 (J43), Siglec-H–Alexa Fluor 647 (ebio440c; all eBioscience); and Sema4a-FITC (5E3; MBL). DAPI (DakoCytomation), 7-AAD (eBioscience), or Zombie NIR (BioLegend) were used to exclude dead cells. For intracellular staining, cells were fixed and permeabilized using the BD Cytofix/Cytoperm kit as per the manufacturer's instructions (BD Biosciences) and stained with FoxP3–Alexa Fluor 647 (MF23; BD Biosciences). For BrdU staining, MLN cells were incubated with 300 µg/ml DNase I (Roche) in PBS at 37°C, followed by washing and staining with anti–BrdU-FITC (BU20A; eBioscience). Stained cells were washed and acquired using a LSRFortessa X-20 Flow Cytometer (BD Biosciences) and analyzed using FACS Diva software v.8 (BD Biosciences) and FlowJo v.8.8 (Tree Star). Antigen-presenting cell populations were gated as previously described (Plantinga et al., 2013), and Sema4a expression was calculated as fold increase in median fluorescence intensity over the fluorescence minus one control.

Cell sorting and culture

For adoptive transfer experiments, T reg cells (Nrp-1$^+$, CD4$^+$, FoxP3-RFP$^+$) were isolated from the MLN of PVM-infected FoxP3-RFP mice at 7 dpi. Single-cell suspensions were generated by digestion of the tissue using a gentleMACS (Miltenyi Biotec) as per the manufacturer's instructions, and RBCs were lysed with Gey's buffer. Cells were washed, blocked with Fc Block, enriched using the EasySep Mouse CD4$^+$ T Cell Isolation kit (StemCell Technologies) and stained with fluorochrome-labeled antibodies as described in the Flow cytometry section. Zombie-NIR$^-$, Nrp-1$^+$, CD4$^+$, FoxP3-RFP$^+$ T reg cells and Zombie-NIR$^-$, CD4$^+$, FoxP3-RFP$^-$ T con cells were sorted on a BD FACSAria Fusion. The purity of FACS-sorted cells was >95% in all cases. 3×10^4 cells or vehicle diluent (10% FCS/DMEM) were adoptively transferred (i.p.) to individual neonate pDC$^\Delta$ or WT mice the same day.

For DC, alveolar macrophage, and T cell co-culture experiments, lung, BAL, and MLN cells were harvested from WT neonatal mice at 7 dpi, and single-cell suspensions were generated by gentle dissociation through a 70-µm cell strainer or GentleMACS. To isolate DCs or alveolar macrophages, CD11c$^+$ cells were enriched using the EasySep Mouse CD11c Positive Selection kit II (StemCell Technologies) followed by FACS sorting of pDCs (Lin$^-$, MHCII$^+$, F4/80$^-$, CD11b$^-$, Siglec-H$^+$), moDCs (Lin-, MHCII$^+$, CD11b$^+$, CD64$^+$, F4/80$^-$), cDCs (Lin$^-$, MHCII$^+$, CD11b$^+$, CD64$^-$, F4/80$^-$), and alveolar macrophages (Lin$^-$, MHCII$^+$, CD11b$^-$, F4/80$^+$). To isolate CD4$^+$ T cells from the MLN of PVM-infected pDC$^\Delta$ neonatal mice, single-cell suspensions were generated, and CD4$^+$ T cells were enriched by MACS as described earlier in this section for T cells, before being stained with 5 µM CFSE (37°C for 10 min) and washed three times. APCs (5×10^3) and CFSE-labeled CD4$^+$ T cells (2×10^5) were seeded into a 96-well round-bottom plates and cultured for 96 h in standard murine growth medium (5×10^{-5} mol/liter RPMI 1640, 10% heat-inactivated FCS, 2 mmol/liter L-glutamine, 20 mmol/liter Hepes, 100 mg/ml penicillin, 100 mg/ml streptomycin, and 0.1 mmol/liter sodium pyruvate) with 1 µg/ml CD3 and 100 U/ml IL-2 in the presence of either anti-Sema4a (757129; R&D Systems) or an isotype control (IgG2a; R&D Systems).

For whole MLN assays, single-cell suspensions of MLN cells from PVM-challenged mice were cultured at 5×10^5 cells/well per 200 µl of growth medium (as before) for 3 d. Supernatants were analyzed by ELISA.

Gene expression analysis

The superior right lobe was excised, stored at 4°C overnight in RNAlater solution (Ambion), and transferred to −80°C. Total RNA was extracted using TriReagent solution (Ambion), and DNase digestion was performed using Turbo DNase (Ambion) according to the manufacturer's instructions. Reverse transcription was performed using M-MLV reverse transcription and random primers (Invitrogen). Quantitative real-time PCR was performed with SYBR Green (Applied Biosystems) as per the manufacturer's instructions. Primer sequences were as follows: *Hprt*, forward 5′-AGGCCAGAC TTTGTTGGATTTGAA-3′ and reverse 5′-CAACTTGCG CTCATCTTAGGCTTT-3′; *Sema4a*, forward 5′-GACGAT GGCAACACTCTCTATG-3′ and reverse 5′-GGCCAG GGTATCATGTTCTTT-3′. Gene expression was calculated using the $-\Delta\Delta$Ct method relative to the housekeeping gene *Hprt* and expressed as fold change compared with naive mice of the respective genotype.

Cytokine and PVM-specific IgG analysis

The concentration of mouse IFN-α (limit of detection [LOD] 2.38 pg/ml; PBL Interferon Source); TNF-α (LOD 5 pg/ml; eBioscience); active IL-10 (LOD 5 pg/ml), IFN-γ (LOD 4 pg/ml), IL-6 (LOD 2 pg/ml), IL-17A (LOD 8 pg/ml; all BioLegend); IL-33 (LOD 14.3 pg/ml) and KC/CXCL1 and eotaxin 2/CCL24 (LOD 15.6 pg/ml; all R&D Systems); IL-4 (LOD 2 pg/ml), IL-5 (LOD 7 pg/ml), IL-13 (LOD 0.274 pg/ml; all BD Bioscience) was quantified in the BALF or lung homogenate by ELISA or cytometric bead array (IL-13 only) as per the manufacturer's instructions. PVM-specific IgG titers were detected in mouse sera using a SMART-spot ELISA kit, according to the manufacturer's instructions (Biotech Trading Partners). The concentration of human IL-6 and IL-10 (LOD 3.91 pg/ml for both) was quantified in the nasal secretions using an in-house ELISA, as described previously (Pritchard et al., 2012).

Immunohistochemistry and histology

Paraffin-embedded sections were prepared as previously described (Davidson et al., 2011). For immunostaining, blocking was performed with 10% normal goat serum or 10% rabbit serum in PBS for 30 min and washed in PBS-Tween 20. Primary antibodies against the PVM G protein (gift from U. Buchholz, National Institutes of Health, Bethesda, MD), FoxP3 (FJK-16s; eBioscience), periostin (Stiny-1; AdipoGen). and α-smooth muscle actin (1A4; Sigma-Aldrich) were incubated overnight at 4°C. Sections were washed three times in PBS/0.05% Tween-20 before incubation with biotinylated anti-mouse polyclonal antibody (Invitrogen; for PVM detection), goat anti–rabbit IgG-AP (Sigma-Aldrich; periostin), or goat anti–mouse IgG-AP (Sigma-Aldrich; α-smooth muscle actin). After 60-min incubation at room temperature, sections were washed three times, and immunoreactivity was developed with Fast Red (Sigma-Aldrich) and counterstained with Gill's hematoxylin before mounting with Glycergel (DakoCytomation). Digitally scanned sections were analyzed using Image Scope Software (Scanscope XT; Aperio). The number of positively PVM-stained APCs was quantified and expressed as a percentage of APCs of five airways. The total number of FoxP3$^+$ cells in the lung parenchyma was counted and expressed as the total number of immunoreactive cells per square millimeter. For quantification of periostin staining, the length of positive staining below the basement membrane was expressed as a percentage of the total circumference of

the basement membrane of five airways per mouse. Sloughing of the airway epithelium was quantified by measuring the length of sloughed airway epithelium and expressing this as a percentage of the basement membrane length of a single airway in at least five airways per mouse. Mucus was identified by periodic acid–Schiff staining and quantified as the length of intraluminal mucus within the inner airway lumen as a percentage of the airway circumference. ASM mass and collagen deposition around the small airways (defined as a circumference <500 µm for neonates and <800 µm for mice >7 wk old) was measured using Scanscope XT software and expressed as area per micrometer of basement membrane. Images were captured at 40× or 100× magnification with an Olympus microscope (model BX51), a digital camera (Olympus DP70), and DP software (Olympus).

Measurement of AHR

Mice were mechanically ventilated, and AHR to inhaled β-methacholine was determined by alterations in resistance by forced oscillation technique as described previously (Phipps et al., 2009). In brief, anesthetized animals were tracheotomized and applied to the Flexivent (SCIREQ). Dose responses to nebulized methacholine (0.3–10 mg/ml; Sigma-Aldrich) were expressed as the percentage change over saline control (baseline).

Human subjects, nasal swabs, and ethics statement

Samples were prospectively collected from 2-yr-old children (interquartile range 1.25–3.86) presenting with acute respiratory infection to the Princess Margaret Hospital Emergency Department as detailed in Table S1. Samples were obtained from previously healthy children as part of an influenza vaccine effectiveness study (Blyth et al., 2014, 2016). Ethical approval for the study was obtained from the ethics committees of Princess Margaret Hospital for Children (1761EP), the South Metropolitan Area Health Service, and the Western Australian Aboriginal Health Information and Ethics Committee. Bilateral mid-turbinate nasal swabs were collected using flocked swabs (Copan Diagnostics). The swab was gently inserted into the nostril until resistance was felt. The swab was rotated several times against the nasal wall. On removal, swabs were inserted into a commercial viral transport media (UTMTM Viral Transport Media; Copan Diagnostics). All samples were frozen at −80°C. Nasopharyngeal samples were tested by PCR for respiratory viruses including RSV.

Bacterial DNA isolation from feces and amplicon sequencing

Bacterial DNA was isolated using the repeated bead beating plus column (RBB+C) method as previously described (Yu and Morrison, 2004). In brief, fecal pellets were collected in screwcap DNase/RNase-free tubes containing 1 ml lysis buffer (500 mM NaCl, 50 mM Tris-HCl, pH 8.0, 50 mM EDTA, and 4% SDS) and 0.4 g sterile zirconia beads (0.3 g of 0.1 mm and 0.1 g of 0.5 mm). The mix was homogenized for 3 min on a Mini-Beedbeater (BioSpec Products). The homogenate was incubated at 70°C for 15 min with gentle shaking, followed by centrifugation at 4°C for 5 min at 16,000 *g* and transfer to a fresh 2-ml Eppendorf tube. Genomic DNA was extracted from the supernatant using the Maxwell LEV Blood DNA kit as per the manufacturer's instructions (Promega). DNA quality was assessed by agarose gel electrophoresis and spectrophotometry (ND-1000; NanoDrop Technologies) or fluorometry (Qubit; Life Technologies). The 16S rRNA gene-based libraries were prepared for sequencing using the MiSeq system (Illumina) according to the manufacturer's instructions. In brief, the V6–V8 region of the 16S rRNA gene was PCR amplified using the 926F and 1492R primers modified to include overhang adapters compatible with the Nextera Index PCR XT kit. Each PCR product was purified using Agencourt AMPure XP beads, and a subsequent PCR was performed using the Nextera Index PCR XT kit with N7XX and S5XX primers. Each PCR product was again purified using Agencourt AMPure XP beads, quantified, normalized, and then pooled in equal quantities. The 16S rRNA gene-based libraries were sequenced at the Australian Centre for Ecogenomics (Brisbane, QLD, Australia).

Sequence processing and data collection

The sequences were analyzed using the Quantitative Insights Into Microbial Ecology (QIIME) software package on an Ubuntu Linux virtual machine (v.5.0.12). In brief, QIIME was used to demultiplex and perform quality control of the sequence data, and only high-quality full-length sequences were further analyzed. The sequences were then clustered into operational taxonomic units (OTUs) using a 97% cutoff with the open reference OTU picking method, in which individual sequences were assigned to their respective OTUs according to the Greengenes database. An OTU table containing taxonomic and abundance data was generated for each individual sample, and OTUs that were not identified as bacteria or archaea and/or OTUs that comprised ≤0.01% of the total sample sequence count were removed. The coverage of each sample was assessed by rarefaction, and a normalized subsampled OTU table was generated by random sampling to the minimum. The subsampled OTU table was used to generate taxonomy plots from phylum to genus levels and calculate α and β diversities.

SCFA analysis

A known volume of ∼100 µl serum was diluted with ultrapure water to a final volume of 200 µl. For fecal samples, 0.1 g feces was broken apart in 200 µl ultrapure water using a pipette tip and vortexed for 45 s. Both serum and fecal extracts were passed through 0.22-µm filters, and SCFA content was determined by injecting 100-µl solute mixed with 11 µl of 10% formic acid into a gas chromatograph fitted with a polar capillary column (DB-FFAP) at 140°C and a flame ionization detector at 250°C (Greenberg et al., 1992).

Statistical analyses

Statistical analyses were performed using GraphPad Prism v.5.0 with Mann–Whitney *U* test for nonparametric data or

Student's *t* test for parametric data as appropriate. When more than two groups were compared, data were analyzed using a one- or two-way ANOVA with Bonferroni post hoc test as appropriate. Correlations were evaluated using a Spearman rank correlation analysis. A p-value <0.05 was considered statistically significant.

Online supplemental material

Fig. S1 shows the gating strategy for pDCs; pDC numbers in lung and MLN at 0 and 10 dpi; quantitation of antiviral, Th1, Th2, and Th17 cytokines, viral load, neutrophils, and eosinophils in the airways; and CD4 and CD8 T cell numbers in lung and MLN. Fig. S2 shows Th1, Th2, and Th17 cytokine levels in MLN cultures and BALF at 49 dpi, quantitation of periostin immunoreactivity in lung at 49 dpi, enumeration of IL-13 (dsRed)– and IL-4 (AmCyan)–producing cells in lung and MLN at 49 dpi, and pathological features of asthma at 42 dpi. Fig. S3 shows RDA plots of microbial communities in feces, SCFA levels in nasal aspirates from children with viral and nonviral bronchiolitis, the study design for SCFA administration to neonatal mice, and quantitation of propanoic acid (serum), IFN-α (BALF), and pDCs (lung) in neonatal mice. Table S1, included as an Excel file, shows the demographics, symptoms, and viruses detected in patients with viral bronchiolitis and symptomatic subjects with no virus detected.

ACKNOWLEDGMENTS

The authors thank the Translational Research Institute Flow Cytometry Facility (Brisbane, Australia) for technical assistance, Dr. Marco Colonna for providing BDAC2-DTR mice, and Dr. Christian Engwerda for providing FoxP3-RFP mice.

This work was supported by a National Health and Medical Research Council grant (1023756) awarded to S. Phipps and J.W. Upham, and an Australian Research Council Future Fellowship (FT130100518) to S. Phipps, an Australian Infectious Diseases Research Centre Excellence Award to J.P. Lynch, J.W. Upham, and S. Phipps, a University of Queensland Microbiome Challenge Award to P.Ó Cuív and M. Morrison, and an equipment grant from the Rebecca L. Cooper Medical Research Foundation.

The authors declare no competing financial interests.

Author contributions: J.P. Lynch and S. Phipps conceived the project, designed the experiments, analyzed and interpreted the data, and prepared the manuscript. J.P. Lynch, R.B. Werder, Z. Loh, M.A.A. Sikder, B. Curren, V. Zhang, M.J. Rogers, K. Lane, J. Simpson, and C. Forstner performed the in vivo experiments. S.B. Mazzone, K. Spann, J. Hayball, K. Diener, M.L. Everard, C.C. Blyth, P.G. Dennis, A. Haque, G.R. Hill, P.D. Sly, and J.W. Upham provided intellectual input and reagents. N. Murtaza, M. Morrison, and P.Ó Cuív performed the microbiota profiling experiments. P. Zhang provided expertise and assisted in the DC and T cell co-culture experiments. G.R. Hill provided reagents and expertise for cell sorting FACS and MACS. M.L. Everard and C.C. Blyth collected the human samples.

Submitted: 15 February 2017
Revised: 21 August 2017
Accepted: 27 November 2017

REFERENCES

Abrahamsson, T.R., H.E. Jakobsson, A.F. Andersson, B. Bjorksten, L. Engstrand, and M.C. Jenmalm. 2014. Low gut microbiota diversity in early infancy precedes asthma at school age. *Clin. Exp. Allergy.* 44:842–850. https://doi.org/10.1111/cea.12253

Arpaia, N., C. Campbell, X. Fan, S. Dikiy, J. van der Veeken, P. deRoos, H. Liu, J.R. Cross, K. Pfeffer, P.J. Coffer, and A.Y. Rudensky. 2013. Metabolites produced by commensal bacteria promote peripheral regulatory T-cell generation. *Nature.* 504:451–455. https://doi.org/10.1038/nature12726

Arrieta, M.-C., L.T. Stiemsma, P.A. Dimitriu, L. Thorson, S. Russell, S. Yurist-Doutsch, B. Kuzeljevic, M.J. Gold, H.M. Britton, D.L. Lefebvre, et al. 2015. Early infancy microbial and metabolic alterations affect risk of childhood asthma. *Sci. Transl. Med.* 7:307ra152. https://doi.org/10.1126/scitranslmed.aab2271

Bendelja, K., A. Gagro, A. Baće, R. Lokar-Kolbas, V. Kršulović-Hrešić, V. Drazenović, G. Mlinaric-Galinović, and S. Rabatić. 2000. Predominant type-2 response in infants with respiratory syncytial virus (RSV) infection demonstrated by cytokine flow cytometry. *Clin. Exp. Immunol.* 121:332–338. https://doi.org/10.1046/j.1365-2249.2000.01297.x

Blyth, C.C., P. Jacoby, P.V. Effler, H. Kelly, D.W. Smith, C. Robins, G.A. Willis, A. Levy, A.D. Keil, and P.C. Richmond. WAIVE Study Team. 2014. Effectiveness of trivalent flu vaccine in healthy young children. *Pediatrics.* 133:e1218–e1225. https://doi.org/10.1542/peds.2013-3707

Blyth, C.C., P. Jacoby, P.V. Effler, H. Kelly, D.W. Smith, M.L. Borland, G.A. Willis, A. Levy, A.D. Keil, and P.C. Richmond. WAIVE Study Team. 2016. Influenza vaccine effectiveness and uptake in children at risk of severe disease. *Pediatr. Infect. Dis. J.* 35:309–315. https://doi.org/10.1097/INF.0000000000000999

Caballero, M.T., M.E. Serra, P.L. Acosta, J. Marzec, L. Gibbons, M. Salim, A. Rodriguez, A. Reynaldi, A. Garcia, D. Bado, et al. 2015. TLR4 genotype and environmental LPS mediate RSV bronchiolitis through Th2 polarization. *J. Clin. Invest.* 125:571–582. https://doi.org/10.1172/JCI75183

Christiaansen, A.F., M.A. Syed, P.P. Ten Eyck, S.M. Hartwig, L. Durairaj, S.S. Kamath, and S.M. Varga. 2016. Altered Treg and cytokine responses in RSV-infected infants. *Pediatr. Res.* 80:702–709. https://doi.org/10.1038/pr.2016.130

Davidson, S., G. Kaiko, Z. Loh, A. Lalwani, V. Zhang, K. Spann, S.Y. Foo, N. Hansbro, S. Uematsu, S. Akira, et al. 2011. Plasmacytoid dendritic cells promote host defense against acute pneumovirus infection via the TLR7-MyD88-dependent signaling pathway. *J. Immunol.* 186:5938–5948. https://doi.org/10.4049/jimmunol.1002635

de Heer, H.J., H. Hammad, T. Soullié, D. Hijdra, N. Vos, M.A. Willart, H.C. Hoogsteden, and B.N. Lambrecht. 2004. Essential role of lung plasmacytoid dendritic cells in preventing asthmatic reactions to harmless inhaled antigen. *J. Exp. Med.* 200:89–98. https://doi.org/10.1084/jem.20040035

Delgoffe, G.M., S.R. Woo, M.E. Turnis, D.M. Gravano, C. Guy, A.E. Overacre, M.L. Bettini, P. Vogel, D. Finkelstein, J. Bonnevier, et al. 2013. Stability and function of regulatory T cells is maintained by a neuropilin-1-semaphorin-4a axis. *Nature.* 501:252–256. https://doi.org/10.1038/nature12428

Edwards, C.L., V. Zhang, R.B. Werder, S.E. Best, I. Sebina, K.R. James, R.J. Faleiro, F. de Labastida Rivera, F.H. Amante, C.R. Engwerda, et al. 2015. Coinfection with blood-stage plasmodium promotes systemic type I interferon production during pneumovirus infection but impairs inflammation and viral control in the lung. *Clin. Vaccine Immunol.* 22:477–483. https://doi.org/10.1128/CVI.00051-15

Feldman, A.S., Y. He, M.L. Moore, M.B. Hershenson, and T.V. Hartert. 2015. Toward primary prevention of asthma. Reviewing the evidence for early-life respiratory viral infections as modifiable risk factors to prevent childhood asthma. *Am. J. Respir. Crit. Care Med.* 191:34–44. https://doi.org/10.1164/rccm.201405-0901PP

Furusawa, Y., Y. Obata, S. Fukuda, T.A. Endo, G. Nakato, D. Takahashi, Y. Nakanishi, C. Uetake, K. Kato, T. Kato, et al. 2013. Commensal microbe-derived butyrate induces the differentiation of colonic regulatory T cells. *Nature.* 504:446–450. https://doi.org/10.1038/nature12721

Gollwitzer, E.S., S. Saglani, A. Trompette, K. Yadava, R. Sherburn, K.D. McCoy, L.P. Nicod, C.M. Lloyd, and B.J. Marsland. 2014. Lung microbiota promotes tolerance to allergens in neonates via PD-L1. *Nat. Med.* 20:642–647. https://doi.org/10.1038/nm.3568

Greenberg, A.E., L.S. Clescerl, and A.D. Eaton, editors. 1992. Standard Methods for the Examination of Water and Wastewater. American Public Health Association, Washington, DC.

Guerrero-Plata, A., A. Casola, G. Suarez, X. Yu, L. Spetch, M.E. Peeples, and R.P. Garofalo. 2006. Differential response of dendritic cells to human metapneumovirus and respiratory syncytial virus. *Am. J. Respir. Cell Mol. Biol.* 34:320–329. https://doi.org/10.1165/rcmb.2005-0287OC

Hall, C.B. 2001. Respiratory syncytial virus and parainfluenza virus. *N. Engl. J. Med.* 344:1917–1928. https://doi.org/10.1056/NEJM200106213442507

Herbst, T., A. Sichelstiel, C. Schär, K. Yadava, K. Bürki, J. Cahenzli, K. McCoy, B.J. Marsland, and N.L. Harris. 2011. Dysregulation of allergic airway inflammation in the absence of microbial colonization. *Am. J. Respir. Crit. Care Med.* 184:198–205. https://doi.org/10.1164/rccm.201010-1574OC

Hill, D.A., M.C. Siracusa, M.C. Abt, B.S. Kim, D. Kobuley, M. Kubo, T. Kambayashi, D.F. Larosa, E.D. Renner, J.S. Orange, et al. 2012. Commensal bacteria-derived signals regulate basophil hematopoiesis and allergic inflammation. *Nat. Med.* 18:538–546. https://doi.org/10.1038/nm.2657

Hooper, L.V., D.R. Littman, and A.J. Macpherson. 2012. Interactions between the microbiota and the immune system. *Science.* 336:1268–1273. https://doi.org/10.1126/science.1223490

Hornung, V., J. Schlender, M. Guenthner-Biller, S. Rothenfusser, S. Endres, K.K. Conzelmann, and G. Hartmann. 2004. Replication-dependent potent IFN-alpha induction in human plasmacytoid dendritic cells by a single-stranded RNA virus. *J. Immunol.* 173:5935–5943. https://doi.org/10.4049/jimmunol.173.10.5935

Huang, Y., L. Guo, J. Qiu, X. Chen, J. Hu-Li, U. Siebenlist, P.R. Williamson, J.F. Urban Jr., and W.E. Paul. 2015. IL-25-responsive, lineage-negative KLRG1(hi) cells are multipotential 'inflammatory' type 2 innate lymphoid cells. *Nat. Immunol.* 16:161–169. https://doi.org/10.1038/ni.3078

James, K.M., T. Gebretsadik, G.J. Escobar, P. Wu, K.N. Carroll, S.X. Li, E.M. Walsh, E.F. Mitchel, C. Sloan, and T.V. Hartert. 2013. Risk of childhood asthma following infant bronchiolitis during the respiratory syncytial virus season. *J. Allergy Clin. Immunol.* 132:227–229. https://doi.org/10.1016/j.jaci.2013.01.009

Johnson, J.E., R.A. Gonzales, S.J. Olson, P.F. Wright, and B.S. Graham. 2007. The histopathology of fatal untreated human respiratory syncytial virus infection. *Mod. Pathol.* 20:108–119. https://doi.org/10.1038/modpathol.3800725

Kaiko, G.E., Z. Loh, K. Spann, J.P. Lynch, A. Lalwani, Z. Zheng, S. Davidson, S. Uematsu, S. Akira, J. Hayball, et al. 2013. Toll-like receptor 7 gene deficiency and early-life Pneumovirus infection interact to predispose toward the development of asthma-like pathology in mice. *J. Allergy Clin. Immunol.* 131:1331–9.e10. https://doi.org/10.1016/j.jaci.2013.02.041

Kamanaka, M., S.T. Kim, Y.Y. Wan, F.S. Sutterwala, M. Lara-Tejero, J.E. Galán, E. Harhaj, and R.A. Flavell. 2006. Expression of interleukin-10 in intestinal lymphocytes detected by an interleukin-10 reporter knockin tiger mouse. *Immunity.* 25:941–952. https://doi.org/10.1016/j.immuni.2006.09.013

Krishnamoorthy, N., A. Khare, T.B. Oriss, M. Raundhal, C. Morse, M. Yarlagadda, S.E. Wenzel, M.L. Moore, R.S. Peebles Jr., A. Ray, and P. Ray. 2012. Early infection with respiratory syncytial virus impairs regulatory T cell function and increases susceptibility to allergic asthma. *Nat. Med.* 18:1525–1530. https://doi.org/10.1038/nm.2896

Lin, W., N. Truong, W.J. Grossman, D. Haribhai, C.B. Williams, J. Wang, M.G. Martín, and T.A. Chatila. 2005. Allergic dysregulation and hyperimmunoglobulinemia E in Foxp3 mutant mice. *J. Allergy Clin. Immunol.* 116:1106–1115. https://doi.org/10.1016/j.jaci.2005.08.046

Lynch, J.P., S.B. Mazzone, M.J. Rogers, J.J. Arikkatt, Z. Loh, A.L. Pritchard, J.W. Upham, and S. Phipps. 2014. The plasmacytoid dendritic cell: at the cross-roads in asthma. *Eur. Respir. J.* 43:264–275. https://doi.org/10.1183/09031936.00203412

Mansbach, J.M., K. Hasegawa, D.M. Henke, N.J. Ajami, J.F. Petrosino, C.A. Shaw, P.A. Piedra, A.F. Sullivan, J.A. Espinola, and C.A. Camargo Jr. 2016. Respiratory syncytial virus and rhinovirus severe bronchiolitis are associated with distinct nasopharyngeal microbiota. *J. Allergy Clin. Immunol.* 137:1909–1913.e4. https://doi.org/10.1016/j.jaci.2016.01.036

Marsland, B.J., and E.S. Gollwitzer. 2014. Host-microorganism interactions in lung diseases. *Nat. Rev. Immunol.* 14:827–835. https://doi.org/10.1038/nri3769

Martín-Gayo, E., E. Sierra-Filardi, A.L. Corbí, and M.L. Toribio. 2010. Plasmacytoid dendritic cells resident in human thymus drive natural Treg cell development. *Blood.* 115:5366–5375. https://doi.org/10.1182/blood-2009-10-248260

Møller-Larsen, S., M. Nyegaard, A. Haagerup, J. Vestbo, T.A. Kruse, and A.D. Børglum. 2008. Association analysis identifies TLR7 and TLR8 as novel risk genes in asthma and related disorders. *Thorax.* 63:1064–1069. https://doi.org/10.1136/thx.2007.094128

Moon, C., M.T. Baldridge, M.A. Wallace, C.A. D, H.W. Burnham, Virgin, and T.S. Stappenbeck. 2015. Vertically transmitted faecal IgA levels determine extra-chromosomal phenotypic variation. *Nature.* 521:90–93. https://doi.org/10.1038/nature14139

Nair, H., D.J. Nokes, B.D. Gessner, M. Dherani, S.A. Madhi, R.J. Singleton, K.L. O'Brien, A. Roca, P.F. Wright, N. Bruce, et al. 2010. Global burden of acute lower respiratory infections due to respiratory syncytial virus in young children: A systematic review and meta-analysis. *Lancet.* 375:1545–1555. https://doi.org/10.1016/S0140-6736(10)60206-1

Palomares, O., B. Ruckert, T. Jartti, U.C. Kucuksezer, T. Puhakka, E. Gomez, H.B. Fahrner, A. Speiser, A. Jung, W.W. Kwok, et al. 2012. Induction and maintenance of allergen-specific FOXP3+ Treg cells in human tonsils as potential first-line organs of oral tolerance. *J. Allergy Clin. Immunol.* 129:510–520.e9. https://doi.org/10.1016/j.jaci.2011.09.031

Pantoja-Feliciano, I.G., J.C. Clemente, E.K. Costello, M.E. Perez, M.J. Blaser, R. Knight, and M.G. Dominguez-Bello. 2013. Biphasic assembly of the murine intestinal microbiota during early development. *ISME J.* 7:1112–1115. https://doi.org/10.1038/ismej.2013.15

Phipps, S., C.E. Lam, G.E. Kaiko, S.Y. Foo, A. Collison, J. Mattes, J. Barry, S. Davidson, K. Oreo, L. Smith, et al. 2009. Toll/IL-1 signaling is critical for house dust mite-specific helper Th1 and Th2 responses. *Am. J. Respir. Crit. Care Med.* 179:883–893. https://doi.org/10.1164/rccm.200806-974OC

Planer, J.D., Y. Peng, A.L. Kau, L.V. Blanton, I.M. Ndao, P.I. Tarr, B.B. Warner, and J.I. Gordon. 2016. Development of the gut microbiota and mucosal IgA responses in twins and gnotobiotic mice. *Nature.* 534:263–266.

Plantinga, M., M. Guilliams, M. Vanheerswynghels, K. Deswarte, F. Branco-Madeira, W. Toussaint, L. Vanhoutte, K. Neyt, N. Killeen, B. Malissen, et al. 2013. Conventional and monocyte-derived CD11b(+) dendritic cells initiate and maintain T helper 2 cell-mediated immunity to house dust mite allergen. *Immunity.* 38:322–335. https://doi.org/10.1016/j.immuni.2012.10.016

Pritchard, A.L., M.L. Carroll, J.G. Burel, O.J. White, S. Phipps, and J.W. Upham. 2012. Innate IFNs and plasmacytoid dendritic cells constrain Th2 cytokine responses to rhinovirus: A regulatory mechanism with relevance to asthma. *J. Immunol.* 188:5898–5905. https://doi.org/10.4049/jimmunol.1103507

Raiden, S., J. Pandolfi, F. Payasliàn, M. Anderson, N. Rivarola, F. Ferrero, M. Urtasun, L. Fainboim, J. Geffner, and L. Arruvito. 2014. Depletion of circulating regulatory T cells during severe respiratory syncytial virus

infection in young children. *Am. J. Respir. Crit. Care Med.* 189:865–868. https://doi.org/10.1164/rccm.201311-1977LE

Roponen, M., S.T. Yerkovich, E. Hollams, P.D. Sly, P.G. Holt, and J.W. Upham. 2010. Toll-like receptor 7 function is reduced in adolescents with asthma. *Eur. Respir. J.* 35:64–71. https://doi.org/10.1183/09031936.00172008

Rosas-Salazar, C., M.H. Shilts, A. Tovchigrechko, J.D. Chappell, E.K. Larkin, K.E. Nelson, M.L. Moore, L.J. Anderson, S.R. Das, and T.V. Hartert. 2016. Nasopharyngeal microbiome in respiratory syncytial virus resembles profile associated with increased childhood asthma risk. *Am. J. Respir. Crit. Care Med.* 193:1180–1183. https://doi.org/10.1164/rccm.201512-2350LE

Russell, S.L., M.J. Gold, M. Hartmann, B.P. Willing, L. Thorson, M. Wlodarska, N. Gill, M.R. Blanchet, W.W. Mohn, K.M. McNagny, and B.B. Finlay. 2012. Early life antibiotic-driven changes in microbiota enhance susceptibility to allergic asthma. *EMBO Rep.* 13:440–447. https://doi.org/10.1038/embor.2012.32

Schijf, M.A., M.V. Lukens, D. Kruijsen, N.O.P. van Uden, J. Garssen, F.E.J. Coenjaerts, B. Van't Land, and G.M. van Bleek. 2013. Respiratory syncytial virus induced type I IFN production by pDC is regulated by RSV-infected airway epithelial cells, RSV-exposed monocytes and virus specific antibodies. *PLoS One.* 8:e81695. https://doi.org/10.1371/journal.pone.0081695

Schlender, J., V. Hornung, S. Finke, M. Günthner-Biller, S. Marozin, K. Brzózka, S. Moghim, S. Endres, G. Hartmann, and K.K. Conzelmann. 2005. Inhibition of Toll-like receptor 7- and 9-mediated alpha/beta interferon production in human plasmacytoid dendritic cells by respiratory syncytial virus and measles virus. *J. Virol.* 79:5507–5515. https://doi.org/10.1128/JVI.79.9.5507-5515.2005

Sharma, M.D., B. Baban, P. Chandler, D.Y. Hou, N. Singh, H. Yagita, M. Azuma, B.R. Blazar, A.L. Mellor, and D.H. Munn. 2007. Plasmacytoid dendritic cells from mouse tumor-draining lymph nodes directly activate mature Tregs via indoleamine 2,3-dioxygenase. *J. Clin. Invest.* 117:2570–2582. https://doi.org/10.1172/JCI31911

Sheppard, P., W. Kindsvogel, W. Xu, K. Henderson, S. Schlutsmeyer, T.E. Whitmore, R. Kuestner, U. Garrigues, C. Birks, J. Roraback, et al. 2003. IL-28, IL-29 and their class II cytokine receptor IL-28R. *Nat. Immunol.* 4:63–68. https://doi.org/10.1038/ni873

Silver, E., H. Yin-DeClue, K.B. Schechtman, M.H. Grayson, L.B. Bacharier, and M. Castro. 2009. Lower levels of plasmacytoid dendritic cells in peripheral blood are associated with a diagnosis of asthma 6 yr after severe respiratory syncytial virus bronchiolitis. *Pediatr. Allergy Immunol.* 20:471–476. https://doi.org/10.1111/j.1399-3038.2008.00818.x

Smit, J.J., B.D. Rudd, and N.W. Lukacs. 2006. Plasmacytoid dendritic cells inhibit pulmonary immunopathology and promote clearance of respiratory syncytial virus. *J. Exp. Med.* 203:1153–1159. https://doi.org/10.1084/jem.20052359

Swiecki, M., and M. Colonna. 2015. The multifaceted biology of plasmacytoid dendritic cells. *Nat. Rev. Immunol.* 15:471–485. https://doi.org/10.1038/nri3865

Swiecki, M., S. Gilfillan, W. Vermi, Y. Wang, and M. Colonna. 2010. Plasmacytoid dendritic cell ablation impacts early interferon responses and antiviral NK and CD8(+) T cell accrual. *Immunity.* 33:955–966. https://doi.org/10.1016/j.immuni.2010.11.020

Tao, R., E.F. de Zoeten, E. Ozkaynak, C. Chen, L. Wang, P.M. Porrett, B. Li, L.A. Turka, E.N. Olson, M.I. Greene, et al. 2007. Deacetylase inhibition promotes the generation and function of regulatory T cells. *Nat. Med.* 13:1299–1307. https://doi.org/10.1038/nm1652

Tarbell, K.V., L. Petit, X. Zuo, P. Toy, X. Luo, A. Mqadmi, H. Yang, M. Suthanthiran, S. Mojsov, and R.M. Steinman. 2007. Dendritic cell–expanded, islet-specific $CD4^+$ $CD25^+$ $CD62L^+$ regulatory T cells restore normoglycemia in diabetic NOD mice. *J. Exp. Med.* 204:191–201. https://doi.org/10.1084/jem.20061631

Teo, S.M., D. Mok, K. Pham, M. Kusel, M. Serralha, N. Troy, B.J. Holt, B.J. Hales, M.L. Walker, E. Hollams, et al. 2015. The infant nasopharyngeal microbiome impacts severity of lower respiratory infection and risk of asthma development. *Cell Host Microbe.* 17:704–715. https://doi.org/10.1016/j.chom.2015.03.008

Trompette, A., E.S. Gollwitzer, K. Yadava, A.K. Sichelstiel, N. Sprenger, C. Ngom-Bru, C. Blanchard, T. Junt, L.P. Nicod, N.L. Harris, and B.J. Marsland. 2014. Gut microbiota metabolism of dietary fiber influences allergic airway disease and hematopoiesis. *Nat. Med.* 20:159–166. https://doi.org/10.1038/nm.3444

Upham, J.W., G. Zhang, A. Rate, S.T. Yerkovich, M. Kusel, P.D. Sly, and P.G. Holt. 2009. Plasmacytoid dendritic cells during infancy are inversely associated with childhood respiratory tract infections and wheezing. *J. Allergy Clin. Immunol.* 124:707–13.e2. https://doi.org/10.1016/j.jaci.2009.07.009

Wang, H., N. Peters, and J. Schwarze. 2006. Plasmacytoid dendritic cells limit viral replication, pulmonary inflammation, and airway hyperresponsiveness in respiratory syncytial virus infection. *J. Immunol.* 177:6263–6270. https://doi.org/10.4049/jimmunol.177.9.6263

Weiss, J.M., A.M. Bilate, M. Gobert, Y. Ding, M.A. Curotto de Lafaille, C.N. Parkhurst, H. Xiong, J. Dolpady, A.B. Frey, M.G. Ruocco, et al. 2012. Neuropilin 1 is expressed on thymus-derived natural regulatory T cells, but not mucosa-generated induced $Foxp3^+$ T reg cells. *J. Exp. Med.* 209:1723–1742. https://doi.org/10.1084/jem.20120914

Yadav, M., C. Louvet, D. Davini, J.M. Gardner, M. Martinez-Llordella, S. Bailey-Bucktrout, B.A. Anthony, F.M. Sverdrup, R. Head, D.J. Kuster, et al. 2012. Neuropilin-1 distinguishes natural and inducible regulatory T cells among regulatory T cell subsets in vivo. *J. Exp. Med.* 209:1713–1722. https://doi.org/10.1084/jem.20120822

Yatsunenko, T., F.E. Rey, M.J. Manary, I. Trehan, M.G. Dominguez-Bello, M. Contreras, M. Magris, G. Hidalgo, R.N. Baldassano, A.P. Anokhin, et al. 2012. Human gut microbiome viewed across age and geography. *Nature.* 486:222–227.

Yu, Z., and M. Morrison. 2004. Improved extraction of PCR-quality community DNA from digesta and fecal samples. *Biotechniques.* 36:808–812.

Zhou, Y., L.B. Bacharier, M. Isaacson-Schmid, J. Baty, K.B. Schechtman, G. Sajol, K. Wylie, G.A. Storch, M. Castro, and A. Beigelman. 2016. Azithromycin therapy during respiratory syncytial virus bronchiolitis: Upper airway microbiome alterations and subsequent recurrent wheeze. *J. Allergy Clin. Immunol.* 138:1215–1219.e5. https://doi.org/10.1016/j.jaci.2016.03.054